

Solution of the quasi-one-dimensional linearized Euler equations using flow invariants and the Magnus expansion

Ignacio Duran^{1,†} and Stephane Moreau²

¹CERFACS, 42 Avenue Gaspard Coriolis, 31057 Toulouse, France

²Université de Sherbrooke, Sherbrooke, Québec, J1K 2R1, Canada

(Received 25 September 2012; revised 7 January 2013; accepted 21 February 2013;
first published online 16 April 2013)

The acoustic and entropy transfer functions of quasi-one-dimensional nozzles are studied analytically for both subsonic and choked flows with and without shock waves. The present analytical study extends both the compact nozzle solution obtained by Marble & Candel (*J. Sound Vib.*, vol. 55, 1977, pp. 225–243) and the effective nozzle length proposed by Stow, Dowling & Hynes (*J. Fluid Mech.*, vol. 467, 2002, pp. 215–239) and by Goh & Morgans (*J. Sound Vib.*, vol. 330, 2011, pp. 5184–5198) to non-zero frequencies for both modulus and phase through an asymptotic expansion of the linearized Euler equations. It also extends the piecewise-linear approximation of the velocity profile in the nozzle proposed by Moase, Brear & Manzie (*J. Fluid Mech.*, vol. 585, 2007, pp. 281–304) to any arbitrary profile or equivalently any nozzle geometry. The equations are written as a function of three variables, namely the dimensionless mass, total temperature and entropy fluctuations, yielding a first-order linear system of differential equations with varying coefficients, which is solved using the Magnus expansion. The solution shows that both the modulus and the phase of the transfer functions of the nozzle have a strong dependence on the frequency. This holds for both choked flows and subsonic converging–diverging nozzles. The method is used to compare two different nozzle geometries with the same inlet and outlet Mach numbers, showing that, even if the compact solution predicts no differences between the transfer functions of the two nozzles, significant differences are found at non-zero frequencies. A parametric study is finally performed to calculate the indirect to direct noise ratio for a model combustor, showing that this ratio decreases at higher frequencies.

Key words: acoustics, aeroacoustics

1. Introduction

The study of the propagation of acoustic and entropy fluctuations through a one-dimensional nozzle is of great importance when dealing with both combustion noise and thermoacoustic instabilities. Marble & Candel (1977) showed that acoustic and entropy waves generated in the combustion chamber of aircraft or helicopter engines contributed significantly to the total engine noise. Two mechanisms control combustion

† Email address for correspondence: ignacio.duran@cerfacs.fr

noise generation, related to the propagation of these two waves to the outlet: direct noise, generated when acoustic waves traverse the turbine stages, and indirect noise, a mechanism in which entropy waves generate noise when accelerated with the mean flow. This source can contribute significantly to the total noise (Candel 1972; Pickett 1975; Muthukrishnan, Strahle & Neale 1978). Recent studies (Leyko *et al.* 2008; Bake *et al.* 2009; Leyko, Nicoud & Poinso 2009; Howe 2010) have shown that the propagation of waves through non-uniform flows plays a major role in the generation and attenuation of combustion noise.

Similarly, when studying thermoacoustic instabilities in combustion chambers of gas turbines, the propagation of acoustic and entropy waves through the inlet and the outlet of the chamber has a significant effect because it controls impedances seen by the combustion chamber upstream and downstream (Poinso & Veynante 2011). Waves generated by the turbulent flame inside the combustion chamber are reflected at the compressor and turbine stages and interact with the flame. The flame reacts to the acoustic perturbation, generating a fluctuating heat release that will in turn produce more acoustic waves. If this fluctuating heat release and the acoustic waves are in phase, a positive feedback will occur as shown by Rayleigh (1878), Dowling (1997) and Dowling & Stow (2003). This may lead to thermoacoustic instabilities if the energy gain exceeds the losses through the boundaries and other dissipation mechanisms (Gullaud *et al.* 2009). The instability mechanism depends strongly on the boundary conditions of the combustion chamber: the phase of the reflection coefficient will influence the resonance frequency at which the instability occurs, and the modulus will control the rate at which the energy of the instability is lost through the boundaries, determining whether the mode is stable or unstable (Williams 1985; Candel & Poinso 1988; Culick 1988; Dowling 1995).

The propagation of waves through nozzles was first studied by Tsien (1952), who analysed the propagation of acoustic waves through a quasi-one-dimensional nozzle with a spatially linear velocity profile. Marble & Candel (1977) extended this result to consider entropy waves and obtained the wave transfer functions of the nozzle using the compact assumption for both subsonic and choked nozzles, showing that entropy waves generated acoustic perturbations when accelerated through a nozzle. This compact hypothesis considers the axial length of the nozzle to be small compared to the wavelength of the perturbation, limiting the results to low frequencies. The frequency dependence of the transfer functions of the nozzle has been studied using mainly two approaches. The first approach was to consider a specific nozzle geometry. This was done by Marble & Candel (1977), following the work of Tsien (1952) in which the nozzle was assumed to have a linear velocity profile. For this very specific case, an analytical solution was obtained in the form of a hypergeometric differential equation. Moase, Brear & Manzie (2007) extended the non-compact analysis for a choked nozzle with a shock wave, where the steady velocity was approximated as piecewise-linear and computed using the solution of Marble & Candel (1977). For each interval with a linear velocity profile, the hypergeometric equation was solved and coupled to the adjacent intervals to compute the complete solution of the nozzle. A different approach to study the non-compact effect was proposed by Stow, Dowling & Hynes (2002). They used an asymptotic analysis to calculate the first-order correction to the low-frequency hypothesis in the case of a choked nozzle with no specific assumption on the nozzle geometry and used this analysis to obtain an effective nozzle length that corrects the phase prediction of the reflection coefficient. Goh & Morgans (2011a) used this result to extend the effective nozzle length to compute the transmission coefficients of a choked flow.

It has been shown (Duran, Moreau & Poinsot 2013) that subsonic converging–diverging nozzles exhibit strong non-compact effects both in the modulus and in the phase of the transfer functions. Work done by Marble & Candel (1977) and by Moase *et al.* (2007) showed that the modulus of the transfer functions of choked nozzles changes significantly with frequency. When considering gas turbines, the modulus of the reflection coefficient represents the energy loss through the boundary conditions (for thermoacoustic instability applications), and the transfer functions represent the acoustic energy propagated downstream (in combustion noise applications). The objective of this paper is to show that Marble and Candel’s method can be extended analytically to non-zero frequencies, removing the compact nozzle assumption to study the evolution of both modulus and phase of the transfer functions at non-zero frequencies for any geometry and any flow configuration using a new asymptotic expansion method.

Two major assumptions are made in this paper: first, the flow is considered quasi-one-dimensional and only plane waves are considered through the nozzle; and second, the Euler equations are used, neglecting viscous terms. The first hypothesis considers that the nozzle is long compared to its characteristic transverse length (for the flow to remain quasi-one-dimensional), and that the waves satisfy $\lambda > l_y$, where l_y is the characteristic length in the transverse direction and λ the wavelength of the perturbation ($\lambda = c/f$, with c the sound speed and f the frequency). This last condition limits the results to frequencies under the first cut-off frequency of the transverse modes of the nozzle. The second hypothesis assumes that viscous effects occur in a negligible zone of the flow, and it has been used frequently in the literature (Marble & Candel 1977; Stow *et al.* 2002; Moase *et al.* 2007).

The effect of viscosity in the propagation of waves through quasi-one-dimensional flows is twofold. First, the development of a steady boundary layer modifies the mean flow calculated using the Euler equations. This effect can be modelled by considering a displacement length of the boundary layer, which reduces the effective section of the nozzle and changes thereby the mean flow configuration through which waves propagate. This modifies the propagation of waves and therefore the transfer functions. This correction, however, may be very important in certain conditions, as the reduction of cross-sectional area through the displacement length of the boundary layer may lead to a choked flow instead of a subsonic one, for example. The propagation of entropy and acoustic waves through the viscous boundary layer is not modelled through the displacement length, but this can be neglected if the boundary layer is small compared to the characteristic section (no flow separation occurs in the divergent region of the nozzle). The second effect of viscosity is the dissipation of acoustic and entropy waves, which occurs only at large frequencies and is neglected in most acoustic propagation models. In addition to these assumptions, the mean flow is supposed to be unaltered by the acoustic and entropy disturbances: the disturbances propagating through it do not lead to oscillations of the flow regime between subsonic and choked conditions and they induce no flow separation. The interaction of shock waves with the boundary layer and with turbulence, as studied by Ribner (1953, 1954, 1987), is also neglected in this quasi-one-dimensional solution. Regardless of these simplifications, it is interesting to obtain an analytical solution of the quasi-one-dimensional Euler equations using the asymptotic expansion in order to compute the transmission and reflection coefficient of waves through nozzles. This could be later used to provide more realistic boundary conditions for large-eddy simulation of actual complex full annular combustion chambers (Gicquel, Staffelbach & Poinsot 2012) and to predict both combustion instabilities and waves transmitted to the turbine stages.

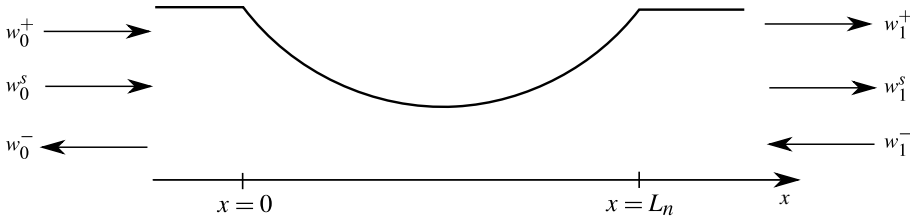


FIGURE 1. Sketch of the acoustic and entropy waves in a subsonic converging–diverging nozzle.

The compact solution of the transfer functions is presented in §2, in which the frequency is assumed to be small. To calculate the solution for any frequency, a general formulation of the problem is proposed in §3, obtaining a first-order linear system of differential equations with varying coefficients. An analytical method to solve the differential equation is presented in §4 using the Magnus expansion initially used to solve the Schrödinger equation (Sakurai & Tuan 1985) and the boundary conditions are discussed in §5. Results and validations versus the linear steady velocity profile nozzle, numerical results and experimental data are illustrated in §6 for different nozzle geometries and configurations; and conclusions are finally discussed in §7.

2. The compact solution

The transfer functions between the upstream and downstream waves of the nozzle were obtained by Marble & Candel (1977) using the compact nozzle assumption, which states that the wavelengths of the acoustic and entropy perturbations are large compared to the axial length of the nozzle. This assumption is therefore valid for low-frequency perturbations only. Using this assumption, acoustic and entropy waves propagate quasi-steadily through the nozzle, and matching conditions can be written between the region upstream of the nozzle (noted with the subscript ‘0’ in figure 1) and the region downstream of the nozzle (noted ‘1’) for the conservative variables mass flow rate, total temperature and entropy. They read

$$\left(\frac{\dot{m}'}{\dot{m}}\right)_0 = \left(\frac{\dot{m}'}{\dot{m}}\right)_1, \quad (2.1)$$

$$\left(\frac{T_t'}{T_t}\right)_0 = \left(\frac{T_t'}{T_t}\right)_1, \quad (2.2)$$

$$\left(\frac{s'}{c_p}\right)_0 = \left(\frac{s'}{c_p}\right)_1, \quad (2.3)$$

where the ‘unaccented’ variables represent the mean steady flow and primed variables $(\)'$ represent small perturbations. To obtain the wave transfer functions, the mass, total temperature and entropy perturbations are first written as functions of three primitive

variables: the dimensionless pressure, velocity and entropy fluctuations, $\varphi = p'/(\gamma p)$, $v = u'/u$ and $\sigma = s'/c_p$. It follows that

$$I_A \equiv \left(\frac{\dot{m}'}{\dot{m}} \right) = \varphi + v - \sigma, \quad (2.4)$$

$$I_B \equiv \left(\frac{T_t'}{T_t} \right) = (\gamma - 1) \frac{M^2 v + \varphi + \frac{\sigma}{\gamma - 1}}{1 + \frac{\gamma - 1}{2} M^2}, \quad (2.5)$$

$$I_C \equiv \left(\frac{s'}{c_p} \right) = \sigma, \quad (2.6)$$

where u and p are the mean flow velocity and pressure respectively, γ is the ratio of specific heats, c_p is the specific heat capacity at constant pressure and $M = u/c$ is the mean flow Mach number, with c the speed of sound. These combinations of primitive variables yield three invariants of the flow, I_A , I_B and I_C , which are conserved through the nozzle when considering the compact nozzle assumption.

When considering a subsonic flow, three boundary conditions can be imposed, corresponding to the downstream-propagating acoustic wave at the inlet (w_0^+), the entropy wave at the inlet (w_0^s) and the upstream-propagating acoustic wave at the outlet (w_1^-) as seen in figure 1. These waves can be expressed as functions of the primitive variables in a non-dimensional form as done by Stow *et al.* (2002), Moase *et al.* (2007) and Leyko *et al.* (2009):

$$w^+ = \varphi + Mv, \quad w^- = \varphi - Mv \quad \text{and} \quad w^s = \sigma. \quad (2.7)$$

Note that these definitions differ from those used by Marble & Candel (1977) by a factor 1/2 in the two acoustic waves, and therefore a factor 1/2 will appear in some terms of the final solution. Using (2.7) in (2.4)–(2.6) and combining them with the jump conditions in (2.1)–(2.3), Marble & Candel (1977) obtained a set of three equations with three unknown outgoing waves and three imposed incoming ones. Considering a unitary incoming entropy wave and no acoustic waves, the entropy transfer functions are obtained and indicate how much acoustic energy is reflected and transmitted by the nozzle when it is hit by an entropy wave. Similarly, the acoustic transfer functions can be calculated by setting $w_0^s = w_1^- = 0$ and a unitary downstream-propagating acoustic wave w_0^+ . The transfer functions for the upstream-propagating acoustic wave at the outlet are obtained by imposing $w_0^s = w_0^+ = 0$. These results are summarized in table 1.

For a choked flow at the throat, the acoustic wave w_1^- at the outlet cannot be imposed, as it propagates downstream. Marble & Candel (1977) imposed the choked flow condition by stating that the fluctuations of the reduced mass flow rate are zero at the inlet. This is equivalent to stating that the Mach number fluctuations are zero at the throat, and using the compact equations (2.1)–(2.3) it is shown that this holds similarly at the nozzle inlet and outlet. The condition can be written as a function of the primitive variables as

$$\frac{M'}{M} = v - \frac{\gamma - 1}{2} \varphi - \frac{\sigma}{2} = 0. \quad (2.8)$$

It should be noted that this condition holds for any frequency at the nozzle throat only, as the Mach number should be 1 at this point and no fluctuations of the Mach

	w_0^-	w_1^+
Response to $w_0^+ = 1$	$\frac{M_1 - M_0}{1 - M_0} \frac{1 + M_0}{M_0 + M_1} \frac{1 - \frac{1}{2}(\gamma - 1)M_0M_1}{1 + \frac{1}{2}(\gamma - 1)M_0M_1}$	$\frac{2M_1}{1 + M_1} \frac{1 + M_0}{M_0 + M_1} \frac{1 + \frac{1}{2}(\gamma - 1)M_1^2}{1 + \frac{1}{2}(\gamma - 1)M_0M_1}$
Response to $w_0^s = 1$	$-\frac{M_1 - M_0}{1 - M_0} \frac{M_0}{1 + \frac{1}{2}(\gamma - 1)M_0M_1}$	$\frac{M_1 - M_0}{1 + M_1} \frac{M_1}{1 + \frac{1}{2}(\gamma - 1)M_0M_1}$
Response to $w_1^- = 1$	$\frac{2M_0}{1 - M_0} \frac{1 - M_1}{M_0 + M_1} \frac{1 + \frac{1}{2}(\gamma - 1)M_0^2}{1 + \frac{1}{2}(\gamma - 1)M_0M_1}$	$-\frac{M_1 - M_0}{1 + M_1} \frac{1 - M_1}{M_0 + M_1} \frac{1 - \frac{1}{2}(\gamma - 1)M_0M_1}{1 + \frac{1}{2}(\gamma - 1)M_0M_1}$

TABLE 1. Compact acoustic and entropy transfer functions in a subsonic nozzle.

	w_0^-	w_1^+	w_1^-
Response to $w_0^+ = 1$	$\frac{1 - \frac{1}{2}(\gamma - 1)M_0}{1 + \frac{1}{2}(\gamma - 1)M_0}$	$\frac{1 + \frac{1}{2}(\gamma - 1)M_1}{1 + \frac{1}{2}(\gamma - 1)M_0}$	$\frac{1 - \frac{1}{2}(\gamma - 1)M_1}{1 + \frac{1}{2}(\gamma - 1)M_0}$
Response to $w_0^s = 1$	$\frac{-M_0}{1 + \frac{1}{2}(\gamma - 1)M_0}$	$\frac{M_1 - M_0}{2(1 + \frac{1}{2}(\gamma - 1)M_0)}$	$\frac{-(M_1 + M_0)}{2(1 + \frac{1}{2}(\gamma - 1)M_0)}$

TABLE 2. Compact acoustic and entropy transfer functions of a choked nozzle.

number can be present. It is only in the compact case that the condition can be shown to hold at any point of the nozzle, which leads to stating that the reduced mass flow rate is choked. Using this extra condition and some algebra, the transfer functions can be calculated for the choked flow and are given in table 2. It is interesting to note that, in the choked case, (2.4), (2.6) and (2.8) lead to the statement that φ , v and σ are constant through the nozzle. Note also that the reflected wave w_0^- does not depend on the outlet Mach number when the flow is choked, as the information on the outlet Mach number cannot travel upstream from the nozzle throat.

The transfer function written hereafter as

$$\left[\frac{w_0^-}{w_0^+} \right] \tag{2.9}$$

represents the upstream acoustic wave, w_0^- , generated at the inlet by a unitary downstream-propagating acoustic wave at the inlet, w_0^+ , and is called the reflection coefficient of the nozzle. The downstream-propagating acoustic wave, w_1^+ , generated by a unitary entropy wave, w_0^s , is simply called the indirect noise (noise generated indirectly by entropy waves).

3. General formulation

To extend the above analytical solution to non-zero frequencies, the quasi-one-dimensional linearized Euler equations (LEEs) are now considered for a calorically

perfect, ideal gas, as in Marble & Candel (1977):

$$\left[\frac{\partial}{\partial t} + u \frac{\partial}{\partial x} \right] \left(\frac{p'}{\gamma p} \right) + u \frac{\partial}{\partial x} \left(\frac{u'}{u} \right) = 0, \quad (3.1)$$

$$\left[\frac{\partial}{\partial t} + u \frac{\partial}{\partial x} \right] \left(\frac{u'}{u} \right) + \frac{c^2}{u} \frac{\partial}{\partial x} \left(\frac{p'}{\gamma p} \right) + \left(2 \frac{u'}{u} - (\gamma - 1) \frac{p'}{\gamma p} - \frac{s'}{c_p} \right) \frac{du}{dx} = 0, \quad (3.2)$$

$$\left[\frac{\partial}{\partial t} + u \frac{\partial}{\partial x} \right] \left(\frac{s'}{c_p} \right) = 0. \quad (3.3)$$

This set of equations is rewritten in dimensionless form, using the dimensionless space and time variables, $\xi = x/L_n$ and $\tau = tf$, where L_n is the nozzle length and f is a characteristic frequency of the perturbation. The mean flow velocity is reduced using the sound speed at the inlet of the nozzle c_0 , giving the dimensionless form $\bar{u} = u/c_0$. The equations are rewritten using the reduced frequency (or Helmholtz number) $\Omega = fL_n/c_0$, which compares the nozzle length with a characteristic acoustic wavelength. In this form the equations read

$$\left[\Omega \frac{\partial}{\partial \tau} + \bar{u} \frac{\partial}{\partial \xi} \right] (\varphi) + \bar{u} \frac{\partial}{\partial \xi} (v) = 0, \quad (3.4)$$

$$\left[\Omega \frac{\partial}{\partial \tau} + \bar{u} \frac{\partial}{\partial \xi} \right] (v) + \frac{\bar{c}^2}{\bar{u}} \frac{\partial}{\partial \xi} (\varphi) + [2v - (\gamma - 1)\varphi - \sigma] \frac{d\bar{u}}{d\xi} = 0, \quad (3.5)$$

$$\left[\Omega \frac{\partial}{\partial \tau} + \bar{u} \frac{\partial}{\partial \xi} \right] (\sigma) = 0. \quad (3.6)$$

Stow *et al.* (2002) and Goh & Morgans (2011a) studied the non-compact response of the choked nozzle performing an asymptotic expansion in Ω , considering $\varphi(x, \Omega) = \varphi^{(0)}(x) + \varphi^{(1)}(x)\Omega + O(\Omega^2)$ and similarly for v and ρ'/ρ , where $()^{(0)}$ stands for the zeroth-order solution of the asymptotic expansion, obtained using the compact theory of Marble & Candel (1977) explained in § 2. Using the fact that the zeroth-order terms are constant through the nozzle in the choked case only, they obtained an analytical expression for the first-order correction and used it to deduce an equivalent nozzle length that corrects the phase of the reflection and transmission coefficients. To extend the analytical solution to subsonic nozzles and to higher-order terms, the asymptotic expansion will be performed to directly correct the compact equations (2.1)–(2.3) instead.

Equations (3.4)–(3.6) are first combined to yield the invariants that were derived from the compact solution of (2.1)–(2.3). To do so, the velocity gradient of the right-hand side of (3.5) is rewritten as a function of the Mach number gradient:

$$\frac{d\bar{u}}{d\xi} = \frac{d}{d\xi}(M\bar{c}) = M \frac{d\bar{c}}{d\xi} + \bar{c} \frac{dM}{d\xi} = \left(\frac{\bar{c}}{1 + \frac{\gamma - 1}{2} M^2} \right) \frac{dM}{d\xi}. \quad (3.7)$$

This result is introduced in (3.5) and then multiplied by M^2 . Rearranging terms, it gives

$$\Omega M^2 \frac{\partial}{\partial \tau} (v) + \bar{u} \frac{\partial}{\partial \xi} (M^2 v + \varphi) - \bar{u} \left(\frac{(\gamma - 1)M}{1 + \frac{\gamma - 1}{2} M^2} \right) \left(M^2 v + \varphi + \frac{\sigma}{(\gamma - 1)} \right) \frac{dM}{d\xi} = 0. \quad (3.8)$$

Combining the spatial derivative terms and using (3.6), the LEEs (3.4)–(3.6) can be rewritten as

$$\Omega \frac{\partial}{\partial \tau} (\varphi - \sigma) + \bar{u} \frac{\partial}{\partial \xi} (\varphi + \nu - \sigma) = 0, \quad (3.9)$$

$$\Omega \frac{\partial}{\partial \tau} \left(M^2 \nu + \frac{\sigma}{(\gamma - 1)} \right) + \bar{u} \left(1 + \frac{\gamma - 1}{2} M^2 \right) \frac{\partial}{\partial \xi} \left(\frac{M^2 \nu + \varphi + \frac{\sigma}{(\gamma - 1)}}{1 + \frac{\gamma - 1}{2} M^2} \right) = 0, \quad (3.10)$$

$$\left[\Omega \frac{\partial}{\partial \tau} + \bar{u} \frac{\partial}{\partial \xi} \right] (\sigma) = 0, \quad (3.11)$$

where no further assumption has been made. Using (2.4)–(2.6) in the limit of small frequencies ($\Omega \rightarrow 0$), the temporal derivatives can be dropped and the compact equations (2.1)–(2.3) are recovered.

To analyse the effects of non-zero frequencies, the equations are written as a function of the invariants I_A , I_B and I_C , introduced in (2.4)–(2.6). These flow invariants are constant through the nozzle at first order for any flow configuration. After some algebra, and writing the substantial derivative as $D/D\tau = \Omega \partial/\partial \tau + \bar{u} \partial/\partial \xi$, the equations read

$$\frac{D}{D\tau} (I_A) = \frac{\bar{u}}{(\gamma - 1)M^2} \left[\frac{\partial}{\partial \xi} (I_C) - \left(1 + \frac{\gamma - 1}{2} M^2 \right) \frac{\partial}{\partial \xi} (I_B) \right], \quad (3.12)$$

$$\frac{D}{D\tau} (I_B) = -\frac{(\gamma - 1)\bar{u}}{1 + \frac{\gamma - 1}{2} M^2} \left[\frac{\partial}{\partial \xi} (I_A) + \frac{\partial}{\partial \xi} (I_C) \right], \quad (3.13)$$

$$\frac{D}{D\tau} (I_C) = 0. \quad (3.14)$$

If the invariants are assumed harmonic, a time Fourier transform (with the $e^{2\pi i \Omega \tau}$ convention) leads to

$$[\mathbf{E}(\xi)] \frac{d}{d\xi} [\mathbf{I}] = 2\pi i \Omega \mathbf{I}, \quad (3.15)$$

where \mathbf{I} is the vector of invariants, containing I_A , I_B and I_C , and $\mathbf{E}(\xi)$ is a non-constant 3×3 matrix,

$$\mathbf{E}(\xi) = -\bar{u} \begin{bmatrix} 1 & \frac{1 + \frac{\gamma - 1}{2} M^2}{(\gamma - 1)M^2} & -\frac{1}{(\gamma - 1)M^2} \\ \frac{\gamma - 1}{1 + \frac{\gamma - 1}{2} M^2} & 1 & \frac{\gamma - 1}{1 + \frac{\gamma - 1}{2} M^2} \\ 0 & 0 & 1 \end{bmatrix}, \quad (3.16)$$

where the Mach number M and the dimensionless speed \bar{u} are functions of the spatial coordinate ξ . When the determinant of \mathbf{E} is non-zero ($M \neq 1$), (3.15) can be inverted,

leading to

$$\frac{d}{d\xi} [\mathbf{I}] = \mathbf{A}(\xi)\mathbf{I}. \quad (3.17)$$

Matrix \mathbf{A} is a non-constant complex matrix of order $O(\Omega)$,

$$\mathbf{A}(\xi) = \frac{-2\pi i \Omega}{\bar{u}(M^2 - 1)} \begin{bmatrix} M^2 & -\frac{1 + \frac{\gamma - 1}{2}M^2}{\gamma - 1} & \frac{\gamma}{\gamma - 1} \\ -(\gamma - 1)M^2 & M^2 & -\frac{(\gamma - 1)M^2 + 1}{1 + \frac{\gamma - 1}{2}M^2} \\ 0 & 0 & M^2 - 1 \end{bmatrix}, \quad (3.18)$$

which represents the correction to the compact hypothesis and where M and \bar{u} are functions of ξ . For choked nozzles, $M = 1$ at the throat, the determinant of \mathbf{E} is zero and the matrix system cannot be inverted. This case will be treated separately in § 5.2.

4. General analytical solution

Stow *et al.* (2002) and Goh & Morgans (2011a) performed an asymptotic expansion in variables φ , v and ρ'/ρ using the fact that the zero-order terms are constant through the nozzle for choked flows. Writing the equation for the first-order correction in the choked case, they found a method to correct the phase of the reflection coefficient through an equivalent nozzle length. In our case the asymptotic expansion can be performed in terms of the invariants (for which the zeroth-order term is constant through the nozzle for any flow configuration): equation (3.17) can be used to obtain an expression for the n th-order term of the asymptotic expansion of \mathbf{I} . Considering $\mathbf{I}(\xi) = \mathbf{I}^{(0)} + \Omega \mathbf{I}^{(1)}(\xi) + \dots + \Omega^n \mathbf{I}^{(n)}(\xi)$, the n th-order equation reads

$$\frac{d}{d\xi} [\mathbf{I}^{(n)}] = \hat{\mathbf{A}}(\xi)\mathbf{I}^{(n-1)} \quad \text{for } n > 0, \quad (4.1)$$

where $\hat{\mathbf{A}} = \mathbf{A}/\Omega$ is independent of Ω because \mathbf{A} is a linear form of Ω as seen in (3.18). This is a similar expression to the one obtained by Stow *et al.* (2002), but written in terms of \mathbf{I} instead of φ , v and ρ'/ρ and generalized up to any order and for any flow configuration. As $\mathbf{I}^{(0)}$ is constant through the nozzle, the first term of the asymptotic expansion can be easily obtained through direct integration of $\hat{\mathbf{A}}(\xi)\mathbf{I}^{(0)}$ element by element. This extends the first-order solution of Stow *et al.* (2002) for any flow condition. Yet, the complexity of this method increases for higher-order terms as $\mathbf{I}^{(n)}$ is in general a function of ξ .

A simpler and more general method is proposed here to solve (3.17) based on the Magnus expansion (Magnus 1954; Blanes *et al.* 2009). In this method, the solution of (3.17) is written as

$$\mathbf{I}(\xi) = [\mathbf{C}(\xi)]\mathbf{I}_0 \quad \text{with } \mathbf{C}(\xi) = \exp(\mathbf{B}(\xi)), \quad (4.2)$$

where \mathbf{I}_0 is the value of the invariant vector at the inlet. The asymptotic expansion is performed in terms of \mathbf{B} instead of expanding \mathbf{I} directly. If matrix $\mathbf{A}(\xi)$ satisfied $\mathbf{A}(\xi_1)\mathbf{A}(\xi_2) - \mathbf{A}(\xi_2)\mathbf{A}(\xi_1) = 0$ for any pair of values ξ_1 and ξ_2 (this is the case, for example, if the Mach number is constant), then matrix $\mathbf{B}(\xi)$ could be calculated

exactly by integrating $\mathbf{A}(\xi)$ term by term,

$$\mathbf{B}(\xi) = \int_0^\xi d\xi_1 \mathbf{A}(\xi_1). \tag{4.3}$$

In a more general case, matrix $\mathbf{B}(\xi)$ is obtained using the Magnus expansion,

$$\mathbf{B}(\xi) = \sum_{k=1}^{\infty} \mathbf{B}^{(k)}(\xi). \tag{4.4}$$

The first three terms are given by

$$\mathbf{B}^{(1)}(\xi) = \int_0^\xi d\xi_1 \mathbf{A}(\xi_1), \tag{4.5}$$

$$\mathbf{B}^{(2)}(\xi) = \frac{1}{2} \int_0^\xi d\xi_1 \int_0^{\xi_1} d\xi_2 [\mathbf{A}(\xi_1), \mathbf{A}(\xi_2)], \tag{4.6}$$

$$\mathbf{B}^{(3)}(\xi) = \frac{1}{6} \int_0^\xi d\xi_1 \int_0^{\xi_1} d\xi_2 \int_0^{\xi_2} d\xi_3 [\mathbf{A}(\xi_1), [\mathbf{A}(\xi_2), \mathbf{A}(\xi_3)]] + [\mathbf{A}(\xi_3), [\mathbf{A}(\xi_2), \mathbf{A}(\xi_1)]], \tag{4.7}$$

where $[\mathbf{A}_1, \mathbf{A}_2] = \mathbf{A}_1\mathbf{A}_2 - \mathbf{A}_2\mathbf{A}_1$ is the matrix commutator. The first term coincides exactly with the solution given in (4.3) for the case when $[\mathbf{A}(\xi_1), \mathbf{A}(\xi_2)] = 0$, and the remaining terms are corrections of higher order. As $\mathbf{A}(\xi)$ is of order $O(\Omega)$, the Magnus expansion verifies that the k th term of the expansion is of order $O(\Omega^k)$. This does not mean that each k th term of the Magnus expansion will only contribute to the k th term of the asymptotic expansion in \mathbf{I} as the exponential of matrix \mathbf{B} should be performed as seen in (4.2).

The terms of the Magnus expansion can be calculated with a recursive procedure, reducing computational costs. Defining the matrix $\mathbf{S}_n^{(k)}$ recursively,

$$\begin{cases} \mathbf{S}_n^{(j)} = \sum_{m=1}^{n-j} [\mathbf{B}^{(m)}, \mathbf{S}_{n-m}^{(j-1)}], & 2 \leq j \leq n-1, \\ \mathbf{S}_n^{(1)} = [\mathbf{B}^{(n-1)}, \mathbf{A}], & \mathbf{S}_n^{(n-1)} = ad_{\mathbf{B}^{(1)}}^{(n-1)}(\mathbf{A}), \end{cases} \tag{4.8}$$

where $ad_{\mathbf{B}}^{(k)}(\mathbf{A})$ is an iterated commutator given by

$$ad_{\mathbf{B}}^{(0)}(\mathbf{A}) = \mathbf{A}, \quad ad_{\mathbf{B}}^{(k+1)}(\mathbf{A}) = [\mathbf{B}, ad_{\mathbf{B}}^{(k)}(\mathbf{A})], \tag{4.9}$$

and $\mathbf{B}^{(k)}$ is finally obtained as

$$\mathbf{B}^{(1)}(\xi) = \int_0^\xi d\xi_1 \mathbf{A}(\xi_1), \tag{4.10a}$$

$$\mathbf{B}^{(n)}(\xi) = \sum_{j=1}^{n-1} \frac{b_j}{j!} \int_0^\xi \mathbf{S}_n^{(j)}(\xi_1) d\xi_1, \tag{4.10b}$$

where b_j are the Bernoulli numbers ($b_1 = -1/2$, $b_2 = 1/6$, $b_3 = 0$, $b_4 = -1/30$, $b_5 = 0$, ...). The Magnus expansion has been widely used to solve linear systems of differential equations with varying coefficients like (4.2), such as in Wilcox (1967) and in Madhu & Kurur (2006).

To obtain the final solution, the value of $\mathbf{B}(\xi)$ has to be computed analytically (if possible) or numerically and its exponential calculated to give \mathbf{C} . This can be done using different methods, as shown in Moler & Van Loan (2003). The method used hereafter is to perform a Taylor series of the exponential, namely,

$$\mathbf{C} = \exp(\mathbf{B}) = \mathbf{I} + (\mathbf{B}) + \frac{1}{2!} (\mathbf{B})^2 + \cdots + \frac{1}{n!} (\mathbf{B})^n. \quad (4.11)$$

Other methods can be used to calculate the matrix exponential with higher accuracy and reducing computational cost. The advantage of the Taylor series used here is that, if the Magnus expansion was truncated at the k th order, the Taylor expansion can also be truncated at the same order (as higher-order terms are meaningless), reducing the complexity of the solution. This method can be used to calculate $\mathbf{C}(\xi)$ in any section. In particular, at the inlet $\mathbf{B}(0) = \mathbf{0}$, and therefore $\mathbf{C}(0) = \mathbf{I}$, the identity matrix.

As each term of the Magnus expansion $\mathbf{B}^{(k)}$ is of order $O(\Omega^k)$, it is possible to calculate a frequency-independent expression of the Magnus expansion using matrix $\hat{\mathbf{A}}$ where the term in Ω has been dropped. This expansion, denoted $\hat{\mathbf{B}}^{(k)}$, is used to obtain a general form with no frequency dependence. When solving for each frequency, the expansion of \mathbf{B} can be calculated as $\mathbf{B} = \sum \Omega^k \hat{\mathbf{B}}^{(k)}$.

The series of (4.4) is an expansion of the solution for $\mathbf{I}(\xi)$ around $\xi = 0$. The series converges fast when the condition given by

$$\int_0^{\xi_F} \|\mathbf{A}(\xi)\|_2 \, d\xi < \pi \quad (4.12)$$

is satisfied (see Moan & Niesen (2006), Casas (2007) and Blanes *et al.* (2009) for more details), but may diverge for larger values of the integral. In the above, $\|\cdot\|_2$ is the 2-norm of the matrix, which for a square matrix is equal to the spectral norm (the largest singular value of the matrix), and can be calculated as

$$\|\mathbf{A}\|_2 = \sqrt{\lambda_{\max}(\mathbf{A}^* \mathbf{A})}, \quad (4.13)$$

where \mathbf{A}^* is the complex conjugate of \mathbf{A} and $\lambda_{\max}(\cdot)$ is the largest eigenvalue of the matrix.

As boundary conditions should be imposed both at the inlet and at the outlet (see § 5), the expansion should be valid until the outlet, $\xi_F = 1$. Integrating (4.12) gives a critical value of the frequency, Ω_{crit} , from which the method may diverge. Below this value, the series converges fast and a few terms are enough to compute an approximate solution.

4.1. Solution for larger frequencies

An analytical solution of the linearized Euler equations has been obtained for frequencies up to Ω_{crit} . This method can be extended to compute the solution up to any frequency as shown in Blanes *et al.* (2009). Given a certain value of Ω_{max} , (4.12) gives the maximal value of $\xi = \xi_1$, for which the solution given by (4.2) converges. In the general case, $\xi_1 < 1$. In that case the remaining part of the solution $\mathbf{I}(\xi)$ may be calculated by expanding it using the Magnus series around ξ_1 , which, for the given value of Ω_{max} , converges until ξ_2 . Proceeding with this method, each Magnus expansion of each nozzle division allows us to write

$$\mathbf{I}(\xi_n) = \exp(\mathbf{B}(\xi_n, \xi_{n-1})) \mathbf{I}(\xi_{n-1}). \quad (4.14)$$

Combining the solutions from the inlet to the outlet,

$$\mathbf{I}(\xi_N) = \prod_{n=1}^N \exp(\mathbf{B}(\xi_n, \xi_{n-1})) \mathbf{I}_0, \tag{4.15}$$

where $\mathbf{B}(\xi_n, \xi_{n-1})$ is the Magnus expansion that relates $\mathbf{I}(\xi_n)$ with $\mathbf{I}(\xi_{n-1})$ through the matrix exponential and N is the number of divisions of the nozzle.

5. Boundary conditions

Once (3.4)–(3.6) are solved, the equations relating the acoustic and entropy perturbations at any point of the nozzle with the perturbations at the inlet are written as $\mathbf{I}(\xi) = \mathbf{C}(\xi) \mathbf{I}_0$. If the compact solution is considered, matrix \mathbf{C} is obtained through (2.1)–(2.6) and is found to be the identity matrix. When considering the general solution in the non-zero-frequency case, \mathbf{C} is frequency-dependent and is calculated with the procedure shown in §4. In both cases, the boundary conditions should provide three equations at the inlet or at the outlet to calculate \mathbf{I}_0 . This should be done imposing only the incoming information. For this reason, vector \mathbf{I} should be decomposed into propagating waves.

To do so, we place ourselves at a region where locally the section is considered constant, at the inlet or at the outlet. Vector \mathbf{I} is written as $\mathbf{I} = \hat{\mathbf{I}} \exp(-i \int_0^\xi \kappa(\zeta) d\zeta)$, with $\hat{\mathbf{I}}$ constant, and introduced in (3.17) to obtain an eigenvalue problem for κ . The solution of this problem leads to

$$\kappa^+ = \frac{2\pi\Omega}{\bar{u} + \bar{c}}, \quad \kappa^- = \frac{2\pi\Omega}{\bar{u} - \bar{c}} \quad \text{and} \quad \kappa^s = \frac{2\pi\Omega}{\bar{u}}, \tag{5.1}$$

which are the wavenumbers of the downstream and upstream acoustic waves and of the entropy wave, propagating at dimensionless speeds $\bar{u} + \bar{c}$, $\bar{u} - \bar{c}$ and \bar{u} , respectively. The associated eigenvectors are obtained and written in a matrix form as

$$\hat{\mathbf{I}} = \mathbf{D}\mathbf{W} = \begin{bmatrix} \eta^+ & \eta^- & -1 \\ \beta^+ & \beta^- & \zeta \\ 0 & 0 & 1 \end{bmatrix} \begin{pmatrix} w^+ \\ w^- \\ w^s \end{pmatrix}, \tag{5.2}$$

where w^+ , w^- and w^s are the acoustic and entropy waves, and

$$\eta^\pm = \frac{1}{2} \left(1 \pm \frac{1}{M} \right), \quad \beta^\pm = \frac{(\gamma - 1)\zeta}{2} (1 \pm M) \quad \text{and} \quad \zeta = \left(1 + \frac{\gamma - 1}{2} M^2 \right)^{-1} \tag{5.3}$$

are used for simplicity. Inverting the system (5.2) and rewriting $\hat{\mathbf{I}}$ using (2.4)–(2.6), the waves can be written as a function of the primitive variables to yield (2.7). Each one of the waves w^+ , w^- and w^s corresponds to a wavenumber κ^+ , κ^- and κ^s , respectively, and therefore to a propagating speed $\bar{u} + \bar{c}$, $\bar{u} - \bar{c}$ and \bar{u} . As only incoming waves can be imposed, a difference should be made between the subsonic and the choked flow.

5.1. Subsonic flow

The propagation speeds of each wave define which ones can be imposed at the boundary condition. For a subsonic flow, the downstream-propagating acoustic wave and the entropy wave are imposed at the inlet (noted with the subscript ‘0’), while the upstream-propagating acoustic wave is imposed at the outlet (noted with ‘1’) as

seen in figure 1. This gives the three conditions that can be imposed to solve for \mathbf{I}_0 . The incoming acoustic waves can be imposed by setting their values either directly, or indirectly through a reflection coefficient, relating it with the outgoing waves. For instance, the downstream-propagating acoustic wave at the inlet can be written as $w_0^+ = w_{0,f}^+ + R_0 w_0^-$, where $w_{0,f}^+$ is a known forcing term at the inlet and R_0 is the acoustic reflection coefficient at the inlet. For the upstream-propagating acoustic wave at the outlet, the expression reads $w_1^- = w_{1,f}^- + R_1 w_1^+ + R_s w_1^s$, where $w_{1,f}^-$ is a known forcing term at the outlet, R_1 is the acoustic reflection coefficient at the outlet and R_s is an extra term that accounts for the generation of upstream-propagating acoustic waves by the entropy waves, which will be used in § 5.2. Similarly, the entropy wave can be written as $w_0^s = w_{0,f}^s + R'_s w_0^-$, where R'_s is the entropy wave generated by an upstream-propagating acoustic wave and will be used in § 5.3. Equation (5.2) is applied at the inlet and at the outlet of the nozzle, where boundary conditions are imposed. Knowing that $\mathbf{I}_1 = \mathbf{C}_1 \mathbf{I}_0$ and using (5.2) for both the inlet and the outlet, the equations for the waves can be written as

$$\mathbf{D}_1 \begin{bmatrix} w^+ \\ w_f^- \\ w^s \end{bmatrix}_1 = \mathbf{C}_1 \mathbf{D}_0 \begin{bmatrix} w_f^+ \\ w^- \\ w_f^s \end{bmatrix}_0, \quad (5.4)$$

where matrices \mathbf{D}_0 and \mathbf{D}_1 are obtained from (5.2) by introducing the additional reflection coefficients,

$$\mathbf{D}_0 = \begin{bmatrix} \eta_0^+ & \eta_0^- + R_0 \eta_0^+ - R'_s & -1 \\ \beta_0^+ & \beta_0^- + R_0 \beta_0^+ + \zeta_0 R'_s & \zeta_0 \\ 0 & R'_s & 1 \end{bmatrix}, \quad (5.5)$$

$$\mathbf{D}_1 = \begin{bmatrix} \eta_1^+ + R_1 \eta_1^- & \eta_1^- & -1 + R_s \eta_1^- \\ \beta_1^+ + R_1 \beta_1^- & \beta_1^- & \zeta_1 + R_s \beta_1^- \\ 0 & 0 & 1 \end{bmatrix}. \quad (5.6)$$

Waves with subscript ‘ f ’ are known (forced at the inlet or at the outlet) and the rest are unknown. There exist several methods to solve this system of equations. Here, a modification of the method proposed by Cumpsty & Marble (1977) to solve the propagation of acoustic and entropy waves through a two-dimensional compact stator vane is adapted to the one-dimensional non-compact nozzle. The matrix system of equation (5.4) can be rearranged to have the unknowns on one side of the equation and the forcing values of the waves on the other side. This is done by exchanging the second column of matrices \mathbf{D}_1 and $\mathbf{C}_1 \mathbf{D}_0$ and changing the sign of each term. This operation leads to an equation $\mathbf{D}_{out} \mathbf{W}_{out} = \mathbf{D}_{in} \mathbf{W}_{in}$, where the vector \mathbf{W}_{in} is composed of the forcing waves $w_{0,f}^+$, $w_{1,f}^-$ and $w_{0,f}^s$, and \mathbf{W}_{out} has the unknown waves w_1^+ , w_0^- and w_1^s . The system can be inverted and solved. If needed, vector \mathbf{I}_0 can then be calculated using (5.2) at the inlet. As matrix \mathbf{C} , and in some cases the reflection coefficients and the forcing waves, are frequency-dependent, the system should be solved individually for each frequency.

5.2. Choked flow

For choked flows, (3.15) cannot be inverted, as the matrix is singular at the throat, where $M = 1$. As (3.15) was obtained through linear combination of (3.4)–(3.6), it can be concluded that these equations present a singularity at the throat of a choked nozzle,

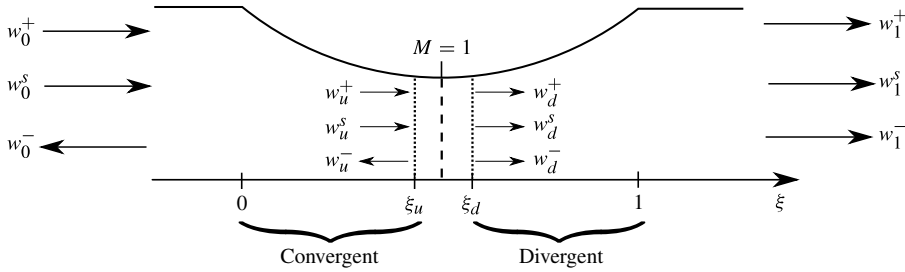


FIGURE 2. Sketch of the acoustic and entropy waves in a converging–diverging choked nozzle.

as shown by Marble & Candel (1977) for the case of a nozzle with a linear velocity profile. This singularity is linked to the upstream-propagating acoustic wave, which changes the propagating direction at the throat. The boundary condition is no longer imposed at the nozzle outlet (as w^- propagates downstream) but at the nozzle throat, where the wave changes sign. The condition that should be imposed is that $M'/M = 0$ at the throat. This condition is equivalent to the one obtained by Stow *et al.* (2002) considering that the solution is regular at the nozzle throat. This condition imposes that, in the choked throat, no fluctuations of the Mach number can be present, as the throat is the region with the minimal section. The condition $M'/M = 0$ can be shifted to the nozzle inlet when considering the compact hypothesis, as done by Marble & Candel (1977), but this cannot be done in the non-compact case, as the boundary condition should be applied at the nozzle throat. It can be shown that for the compact case this condition is the same as the one imposed by Marble & Candel (1977), as explained in § 2

To solve a converging–diverging nozzle with a choked flow, the two sections on both sides of the discontinuity will be calculated separately and matched together, as illustrated in figure 2. First, the convergent subsonic region of the flow is calculated as in § 5.1, imposing two waves at the inlet (w_0^+ and w_0^s) and calculating the upstream-propagating acoustic wave at the outlet (w_u^-) using the condition $M'/M = 0$. Secondly, the supersonic part of the nozzle is calculated, imposing three waves at the inlet, obtained from the solution of the subsonic part and the analysis of the throat region.

To correctly impose the boundary conditions at the outlet of the subsonic half (w_u^-), and to calculate the three waves at the inlet of the supersonic region, the flow through the nozzle throat should be analysed first. A small slab with infinitesimally wide section through the throat is considered, as was done by Moase *et al.* (2007) (as shown in figure 2), in which the Mach numbers at the inlet and at the outlet are $M_u = 1 - \epsilon$ and $M_d = 1 + \epsilon$, respectively, where subscripts u and d denote the quantities taken upstream and downstream of the compact nozzle throat region and $\epsilon \ll 1$. The boundary condition $M'/M = 0$ of (2.8) is applied at the nozzle throat, which is compact in the throat region. It can be shown (Marble & Candel 1977; Stow *et al.* 2002) that, for this compact region, this condition applies at any section of the infinitesimally short nozzle (as seen in § 2). Writing (2.8) at the outlet of the upstream subsonic half-section as a function of the three waves at the inlet (using (2.7)), and taking the limit $\epsilon \rightarrow 0$, the unknown reflected wave w_u^- can be calculated as a function of the two incoming waves,

$$w_u^- = R_u w_u^+ + R_s w_u^s, \tag{5.7}$$

with

$$R_u = \frac{3 - \gamma}{\gamma + 1} \quad \text{and} \quad R_s = \frac{-2}{\gamma + 1}. \quad (5.8)$$

These reflection coefficients R_u and R_s should be imposed at the nozzle throat, and the subsonic part of the nozzle can be solved as in § 5.1.

For the supersonic half, the three waves should be imposed at the inlet using the relation $I_u = I_d$ for the compact region. The invariants at the outlet of the nozzle are calculated using the Magnuss expansion in the supersonic section, and knowing that $I_1 = \mathbf{C}^{(d)} I_d$, where $\mathbf{C}^{(d)}$ is calculated only in the diverging part of the nozzle. Inverting (5.2), the waves at the outlet of the diverging section are calculated.

5.3. Supersonic flow with a shock wave

The transfer functions of a supersonic nozzle with a shock wave can be calculated by dividing the nozzle into two regions: the upstream region from the shock, which is computed as in § 5.2, and the downstream region, calculated with the subsonic solution shown in § 5.1. The shock wave acts as an interface between the two regions. The response of the shock wave to acoustic and entropy perturbations has been studied in depth (Marble & Candel 1977; Kuo & Dowling 1996; Stow *et al.* 2002; Moase *et al.* 2007; Goh & Morgans 2011a; Leyko *et al.* 2011). The main steps of the method are summarized here; the reader is referred to Moase *et al.* (2007) and Goh & Morgans (2011a) for more details.

First of all, the usual Rankine–Hugoniot shock relations are here written for the outlet Mach number, the pressure, density and velocity as a function of the inlet Mach number, as in Stow *et al.* (2002),

$$M_b^2 = \frac{1 + \frac{\gamma - 1}{2} M_a^2}{\gamma M_a^2 - \frac{\gamma - 1}{2}}, \quad (5.9a)$$

$$\frac{p_b}{p_a} = \frac{2\gamma M_a^2 - (\gamma - 1)}{\gamma + 1} \quad (5.9b)$$

and

$$\frac{\rho_b}{\rho_a} = \frac{u_a}{u_b} = \frac{\frac{\gamma + 1}{2} M_a^2}{1 + \frac{\gamma - 1}{2} M_a^2}, \quad (5.9c)$$

where the subscripts $()_a$ and $()_b$ represent quantities taken upstream and downstream of the shock wave, as shown in figure 3. The shock is considered to oscillate about a mean position ξ_s with an amplitude ξ'_s due to the acoustic and entropy perturbations. These oscillations are assumed to be infinitesimally small. This can be ensured if $dA/d\xi > 0$ and is continuous at the shock location. The first-order perturbations of the pressure, density and velocity equations through the shock wave in its reference frame give

$$\frac{p'_{b,sh}}{\gamma p_b} - \frac{p'_{a,sh}}{\gamma p_a} = \frac{4M_a^2}{(\gamma + 1)} \left(\frac{p_a}{p_b} \right) \left(\frac{M'_{a,sh}}{M_a} \right), \quad (5.10a)$$

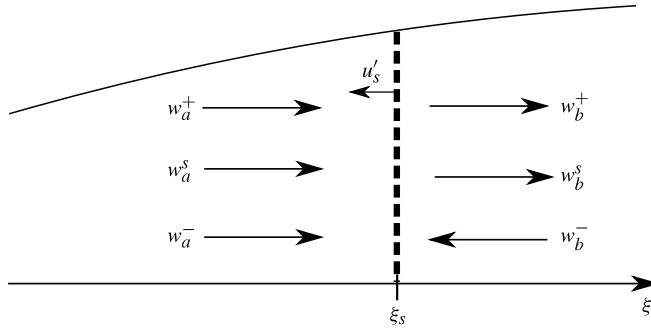


FIGURE 3. Sketch of a shock wave in a diverging section; u'_s is the movement of the shock wave due to the incoming perturbations.

$$\frac{\rho'_{b,sh}}{\rho_b} - \frac{\rho'_{a,sh}}{\rho_a} = \frac{4}{M_a^2(\gamma + 1)} \left(\frac{u_a}{u_b} \right) \left(\frac{M'_{a,sh}}{M_a} \right), \quad (5.10b)$$

$$\frac{u'_{b,sh}}{u_b} - \frac{u'_{a,sh}}{u_a} = \frac{-4}{M_a^2(\gamma + 1)} \left(\frac{u_a}{u_b} \right) \left(\frac{M'_{a,sh}}{M_a} \right). \quad (5.10c)$$

The subscript $()_{sh}$ represents the fluctuations seen by the shock wave in its reference frame, which can be decomposed into two terms: the absolute fluctuation in the fixed reference frame, and an extra term caused by the movement of the shock wave inside a nozzle with a mean pressure/density gradient. Up to first order they read

$$\frac{p'_{a,sh}}{\gamma p_a} = \frac{p'_a}{\gamma p_a} + \frac{\xi'_s}{\gamma p_a} \frac{dp_a}{d\xi}, \quad (5.11a)$$

$$\frac{\rho'_{a,sh}}{\rho_a} = \frac{\rho'_a}{\rho_a} + \frac{\xi'_s}{\rho_a} \frac{d\rho_a}{d\xi}, \quad (5.11b)$$

and similarly downstream of the shock wave. Note that the second term should be included to account for the displacement of the shock wave inside a nozzle with a mean flow gradient. The velocity and Mach number fluctuations seen by the shock wave are written as

$$\frac{u'_{a,sh}}{u_a} = \frac{u'_a}{u_a} + \frac{\xi'_s}{u_a} \frac{du_a}{d\xi} - \frac{1}{\bar{u}_a} \frac{d\xi'_s}{d\tau} = \frac{u'_a}{u_a} + \frac{\xi'_s}{u_a} \frac{du_a}{d\xi} - \frac{2\pi i \Omega}{M_a \bar{c}_a} \xi'_s, \quad (5.12)$$

$$\frac{M'_{a,sh}}{M_a} = \frac{M'_a}{M_a} + \frac{\xi'_s}{M_a} \frac{dM_a}{d\xi} - \frac{1}{M_a \bar{c}_a} \frac{d\xi'_s}{d\tau} = \frac{M'_a}{M_a} + \frac{\xi'_s}{M_a} \frac{dM_a}{d\xi} - \frac{2\pi i \Omega}{M_a \bar{c}_a} \xi'_s, \quad (5.13)$$

where the last term is caused by the movement of the shock wave, and M'_a/M_a is given through (2.8) as a function of the pressure, velocity and entropy fluctuations.

To close the system of equations, the mean pressure and density gradients are written as a function of the mean Mach number gradient using the isentropic relations upstream and downstream of the shock wave. They read

$$\frac{1}{\gamma p} \frac{dp}{d\xi} = \frac{1}{\rho} \frac{d\rho}{d\xi} = \frac{-M}{1 + \frac{\gamma - 1}{2} M^2} \frac{dM}{d\xi}. \quad (5.14)$$

A similar expression was given in (3.7) for the mean velocity gradient. Finally, using the mass conservation through the shock wave, the Mach number gradient downstream can be written as a function of the upstream one,

$$\frac{M_b^2 - 1}{M_b \left(1 + \frac{\gamma - 1}{2} M_b^2\right)} \frac{dM_b}{d\xi} = \frac{M_a^2 - 1}{M_a \left(1 + \frac{\gamma - 1}{2} M_a^2\right)} \frac{dM_a}{d\xi}. \quad (5.15)$$

Using (5.11) and (5.12) in (5.10), and writing the mean pressure, velocity and density gradients as functions of the Mach gradient upstream of the shock wave (using (5.14), (5.15) and (3.7)), the equations for the fluctuating primitive variables upstream and downstream of the nozzle shock read

$$\frac{p'_b}{\gamma p_b} - \frac{p'_a}{\gamma p_a} = \frac{4M_a^2}{(\gamma + 1)} \left(\frac{p_a}{p_b}\right) \left[\frac{M'_a}{M_a} + \Gamma_p \xi'_s\right], \quad (5.16a)$$

$$\frac{\rho'_b}{\rho_b} - \frac{\rho'_a}{\rho_a} = \frac{4}{M_a^2(\gamma + 1)} \left(\frac{u_a}{u_b}\right) \left[\frac{M'_a}{M_a} + \Gamma_\rho \xi'_s\right], \quad (5.16b)$$

$$\frac{u'_b}{u_b} - \frac{u'_a}{u_a} = \frac{-4}{M_a^2(\gamma + 1)} \left(\frac{u_a}{u_b}\right) \left[\frac{M'_a}{M_a} + \Gamma_u \xi'_s\right], \quad (5.16c)$$

where for simplicity the functions Γ are defined as

$$\Gamma_p = \left[1 - \frac{M_b^2 - M_a^2}{2M_a^2 M_b^2 (M_b^2 - 1)}\right] \frac{1}{M_a} \frac{dM_a}{d\xi} - \frac{2\pi i \Omega}{M_a \bar{c}_a}, \quad (5.17a)$$

$$\Gamma_\rho = \frac{1}{2} \left[1 + \frac{M_a^2 - 1}{M_b^2 - 1}\right] \frac{1}{M_a} \frac{dM_a}{d\xi} - \frac{2\pi i \Omega}{M_a \bar{c}_a}, \quad (5.17b)$$

$$\Gamma_u = \frac{1}{2} \left[1 + \frac{M_a^2 - 1}{M_b^2 - 1}\right] \frac{1}{M_a} \frac{dM_a}{d\xi} - \left(\frac{M_a^2 + 1}{2}\right) \frac{2\pi i \Omega}{M_a \bar{c}_a}. \quad (5.17c)$$

The three equations of (5.16) can be combined to obtain two jump conditions independent of ξ'_s . The upstream fluctuating Mach number can be written as a function of the primitive variables using (2.8) and knowing that $\rho'/\rho = \varphi - \sigma$, and using (2.7) the two jump conditions can be written as a function of the upstream- and downstream-propagating acoustic waves and the entropy wave and solved to obtain the transfer functions of table 3.

The downstream subsonic region of the nozzle shock is calculated using the method presented in § 5.1. At the inlet, the acoustic and the entropy waves coming from the shock waves have to be imposed. Using table 3 they read

$$w_b^+ = \underbrace{\left[\frac{w_b^+}{w_a^+}\right] w_a^+ + \left[\frac{w_b^+}{w_a^-}\right] w_a^- + \left[\frac{w_b^+}{w_a^s}\right] w_a^s}_{w_{b,f}^+} + \underbrace{\left[\frac{w_b^+}{w_b^-}\right] w_b^-}_{R_{in}}, \quad (5.18)$$

$$w_b^s = \underbrace{\left[\frac{w_b^s}{w_a^+}\right] w_a^+ + \left[\frac{w_b^s}{w_a^-}\right] w_a^- + \left[\frac{w_b^s}{w_a^s}\right] w_a^s}_{w_{b,f}^s} + \underbrace{\left[\frac{w_b^s}{w_b^-}\right] w_b^-}_{R'_s}. \quad (5.19)$$

The downstream-propagating acoustic wave is composed of a forcing wave $w_{b,f}^+$ corresponding to the first three terms of (5.18) and a reflection coefficient at the inlet

	w_b^+	w_b^s
Response to $w_a^+ = 1$	$\frac{\alpha^+}{\psi^+}$	$\phi \left(\frac{\alpha^+}{\psi^+} - 1 \right) - \Lambda \left(1 - \frac{\gamma - 1}{2} M_a \right)$
Response to $w_a^- = 1$	$\frac{\alpha^-}{\psi^+}$	$\phi \left(\frac{\alpha^-}{\psi^+} - 1 \right) + \Lambda \left(1 + \frac{\gamma - 1}{2} M_a \right)$
Response to $w_a^s = 1$	$M_a^2 M_b^2 \frac{\delta}{\psi^+}$	$1 + M_a^2 M_b^2 \frac{\delta}{\psi^+} + M_a \Lambda$
Response to $w_b^- = 1$	$-\frac{\psi^-}{\psi^+}$	$\phi \left(1 - \frac{\psi^-}{\psi^+} \right)$

$$\Lambda = \frac{1 - \left(\frac{\Gamma_\rho}{\Gamma_p} \right)}{M_a \left(1 + \frac{\gamma - 1}{2} M_a^2 \right)}, \quad \delta = \frac{2 \left(1 - \frac{\Gamma_u}{\Gamma_p} \right)}{\left(1 + \frac{\gamma - 1}{2} M_a^2 \right)}$$

$$\alpha^\pm = \left(\frac{\Gamma_u}{\Gamma_p} \right) \pm M_a M_b^2 \left[1 - \delta \left(1 \mp \frac{\gamma - 1}{2} M_a \right) \right]$$

$$\phi = \frac{1}{2} \left[1 - \frac{1}{M_a^2 M_b^2} \left(\frac{\Gamma_\rho}{\Gamma_p} \right) \right], \quad \psi^\pm = \left(\frac{\Gamma_u}{\Gamma_p} \right) \pm M_a M_b$$

TABLE 3. Acoustic and entropy transfer functions through a shock wave.

equal to the last term. Similarly, the entropy wave imposed at the inlet is divided into a forcing term (the first three terms of (5.19)) and an entropy reflection coefficient R'_s , corresponding to the last term. Using these forcing waves and reflection coefficients, the subsonic region downstream of the shock can be calculated as in § 5.1.

6. Results

The method described in §§ 3–5 is here used to obtain the transfer functions of several nozzle geometries at all frequencies. The asymptotic expansion is performed up to fifth order in Ω , and the nozzle divided into several sections as shown in (4.14) depending on each case. It was shown that, with the nozzle divisions satisfying (4.12), a fifth-order expansion in Ω is enough for the series to converge, and higher-order terms are negligible for all cases considered in the present study. The integrals in the Magnus expansion are calculated using Simpson's rule. In § 6.1 the method is used to calculate a nozzle with a linear steady velocity profile, comparing the result with the analytical solution of Marble & Candel (1977). A more realistic nozzle is also considered to evaluate the influence of the exact Mach number profile on the transfer functions. The analytical model is then compared with the experimental data of Bell, Daniel & Zinn (1973) in § 6.2. In § 6.3 the invariant method is compared with the phase correction of the reflection coefficient through an effective nozzle length proposed by Stow *et al.* (2002) and to the extension proposed by Goh & Morgans (2011a) when considering a choked flow through the nozzle. Section 6.4 focuses on

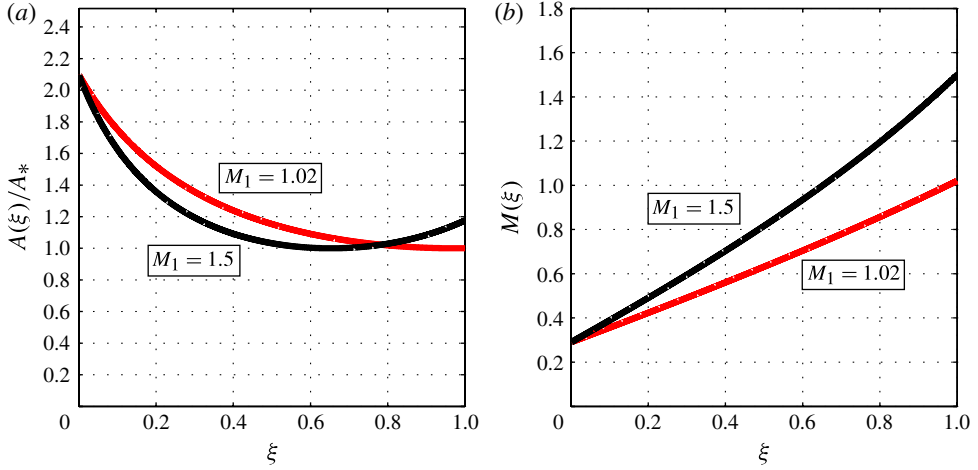


FIGURE 4. (Colour online) Section and Mach number of two linear steady velocity profile nozzles with inlet Mach number of $M_0 = 0.29$ and two different outlet Mach numbers.

the transfer functions of subsonic converging–diverging nozzles. Finally a parametric study on indirect to direct combustion noise is performed in § 6.5 to extend the results of Leyko *et al.* (2009) to non-zero frequencies and provide some insight on how this ratio may vary at the exit of the turbine stage with increasing frequency.

6.1. Comparison with a linear steady velocity choked nozzle

In this subsection the invariant solution is compared with the analytical method proposed by Marble & Candel (1977) for a non-compact nozzle. This method (detailed in the Appendix) is not general. It can be used only by assuming a specific nozzle geometry in which the steady velocity varies linearly with the axial coordinate (hereafter called the linear nozzle for simplicity). Using this assumption, and with an appropriate change of variable, the solution of the linearized Euler equations (3.1)–(3.3) can be written as a sum of hypergeometric functions. Two nozzles are considered here, corresponding to an inlet Mach number of $M_0 = 0.29$ and two different outlet Mach numbers ($M_1 = 1.02$ and $M_1 = 1.5$). The nozzle Mach number profile is calculated using (A 15) as explained in the Appendix and the nozzle section is obtained using the steady quasi-one-dimensional Euler equations and is given by

$$\frac{A}{A_*} = \frac{1}{M} \left[\left(\frac{2}{\gamma + 1} \right) \left(1 + \frac{\gamma - 1}{2} M^2 \right) \right]^{(\gamma+1)/2(\gamma-1)}, \quad (6.1)$$

where A_* is the critical section, where the Mach number is unity (equal in this case to the throat section, as the flow is choked). Figure 4 shows the nozzle section and the Mach number plotted as functions of the non-dimensional nozzle length ξ for both nozzles. The responses of the two nozzles to an entropy perturbation at the inlet are plotted in figure 5 as a function of the reduced frequency Ω . The invariants method and the hypergeometric equations are used to solve both cases, showing that both methods give the same results when the same linear velocity profile is used, and tend to the compact solution for $\Omega = 0$. The indirect noise generated in this configuration decreases with increasing frequency, showing that the compact nozzle hypothesis is limited to low frequencies and that the modulus, and not only the phase, depends

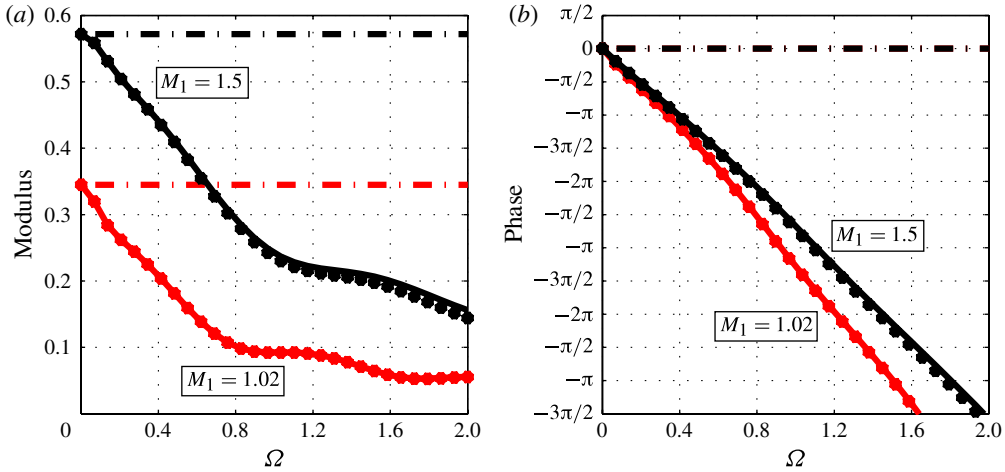


FIGURE 5. (Colour online) Amplitude and phase of the downstream-facing acoustic wave at the outlet w_1^+ generated by an incoming entropy wave, $w_0^s = 1$, with $M_0 = 0.29$. Invariants method (—); hypergeometric equation (●) and compact solution (---).

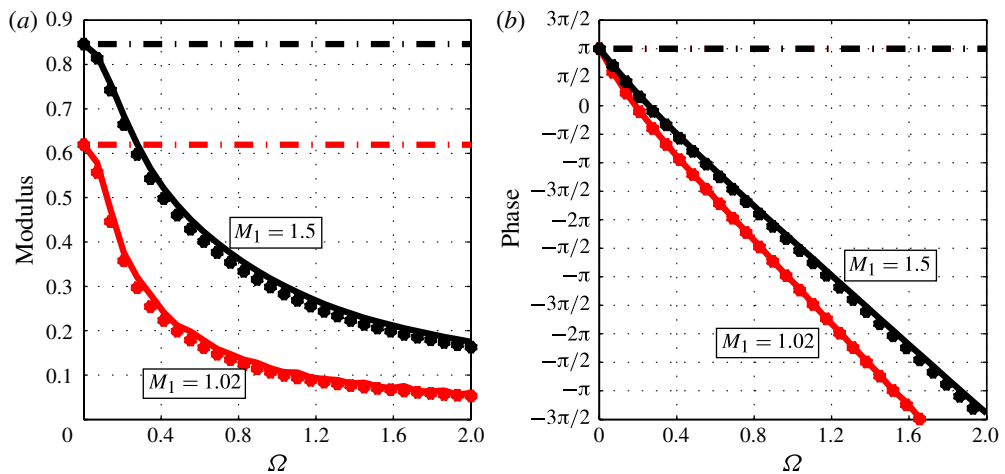


FIGURE 6. (Colour online) Amplitude and phase of the upstream-facing acoustic wave at the outlet w_1^- generated by an incoming entropy wave, $w_0^s = 1$, with $M_0 = 0.29$. Invariants method (—); hypergeometric equation (●) and compact solution (---).

strongly on the frequency. Figure 6 shows the upstream facing propagating acoustic wave at the outlet.

Both the invariant method and the hypergeometric equations can also be used to solve for the reflection coefficient of linear nozzles. In figure 7 the acoustic reflection coefficient of a choked nozzle with $M_0 = 0.29$ and $M_1 = 1.5$ is plotted for a unitary acoustic wave at the inlet. The modulus of the reflected acoustic wave is seen to tend to zero as the frequency increases. Thus, the acoustic energy loss through the outlet boundary increases with frequency, which is of great importance when studying thermoacoustic instabilities. These results show the strong dependence of the transfer

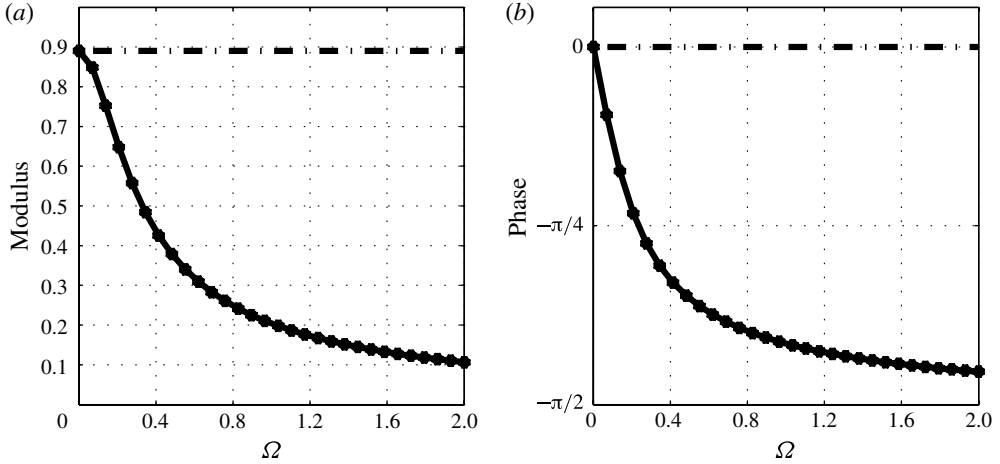


FIGURE 7. Amplitude and phase of the reflection coefficient (w_0^- due to w_0^+) for a linear steady velocity choked nozzle with $M_0 = 0.29$ and $M_1 = 1.5$. Invariants method (—); hypergeometric equation (\bullet) and compact solution ($-\cdot-\cdot-$).

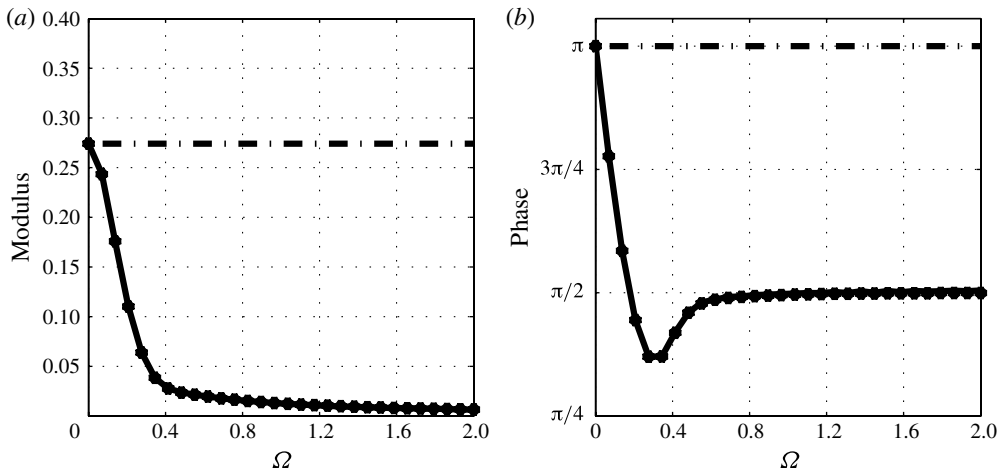


FIGURE 8. Amplitude and phase of the acoustic wave w_0^- generated by an incoming entropy wave, $w_0^s = 1$, with $M_0 = 0.29$ and $M_1 = 1.5$. Invariants method (—); hypergeometric equation (\bullet).

functions on frequency, demonstrating that the compact nozzle hypothesis may not be suited for these applications when considering non-zero frequencies. Figure 8 shows the upstream-propagating acoustic wave at the inlet generated by an entropy wave. This wave is responsible for low-frequency instabilities in combustion chambers, as mentioned by Goh & Morgans (2011b) and already observed in some industrial cases (Motheau *et al.* 2012).

It is interesting to compare the solutions obtained using the linear nozzle with a more realistic geometry. Actual nozzles usually have a long diverging region compared to the converging one. This is generally done to avoid flow separation at the diverging

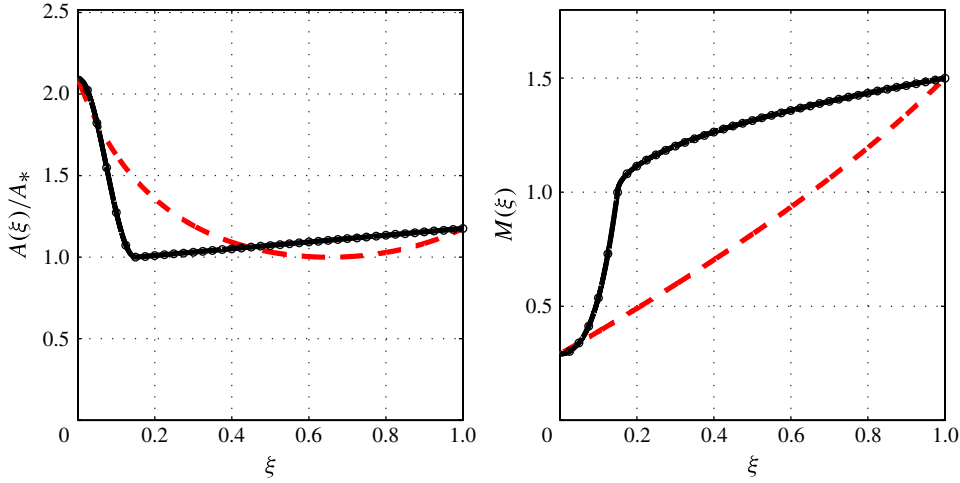


FIGURE 9. (Colour online) Section and Mach number of a converging–diverging nozzle. Geometry obtained with (6.2) (—) and with the linear steady velocity profile (– – –) with inlet and outlet Mach numbers $M_0 = 0.29$ and $M_1 = 1.5$ for both nozzles; (•) represents the nozzle subdivisions for the invariants method to calculate up to $\Omega = 5$.

section, where an adverse pressure gradient exists. When comparing two different geometries with the same inlet and outlet Mach numbers, the compact solution at zero frequency predicts the same values for the transfer functions for both nozzles. This is not the case for non-zero frequencies, where the transfer function depends strongly on the Mach number profile $M(\xi)$, and therefore on the specific geometry considered and not only on the inlet and outlet Mach numbers. The transfer functions of the linear nozzle are therefore compared with those of a more realistic geometry with the same inlet and outlet Mach numbers to evaluate the differences between the transfer functions at non-zero frequencies. The geometry studied here is given by a simple analytical expression dividing the converging and the diverging regions into two parts,

$$\frac{A(\xi)}{A_*} = \begin{cases} \frac{1}{2} \left(\frac{A_0}{A_*} - 1 \right) \left[\cos \left(\pi \frac{\xi}{\xi_*} \right) + 1 \right] + 1 & \text{if } \xi \in [0, \xi_*], \\ 1 + \left(\frac{A_1}{A_*} - 1 \right) \frac{\xi - \xi_*}{1 - \xi_*} & \text{if } \xi \in [\xi_*, 1], \end{cases} \quad (6.2)$$

where $A(\xi)$ is the nozzle section. Subscript $()_*$ represents the throat section where $M_* = 1$. The nozzle is fully described with three parameters: the non-dimensional converging length ($\xi_* = 0.15$ for the rest of this section) and the inlet and outlet dimensionless section ratios A_0/A_* and A_1/A_* , which are related to the inlet and outlet Mach numbers through (6.1). A cosine profile was chosen for the converging region to yield a smooth flow up to the throat, while the diverging section was chosen linear, so that the radius is proportional to \sqrt{x} , which is a usual feature of rocket engines. This allows a complete description of the nozzle with only three parameters. The nozzle geometry and Mach number are shown in figure 9 for the $M_0 = 0.29$, $M_1 = 1.5$ case used here, compared with the previous geometry obtained for the linear nozzle. Note that the diverging region is larger in the realistic nozzle than in the linear one, and that

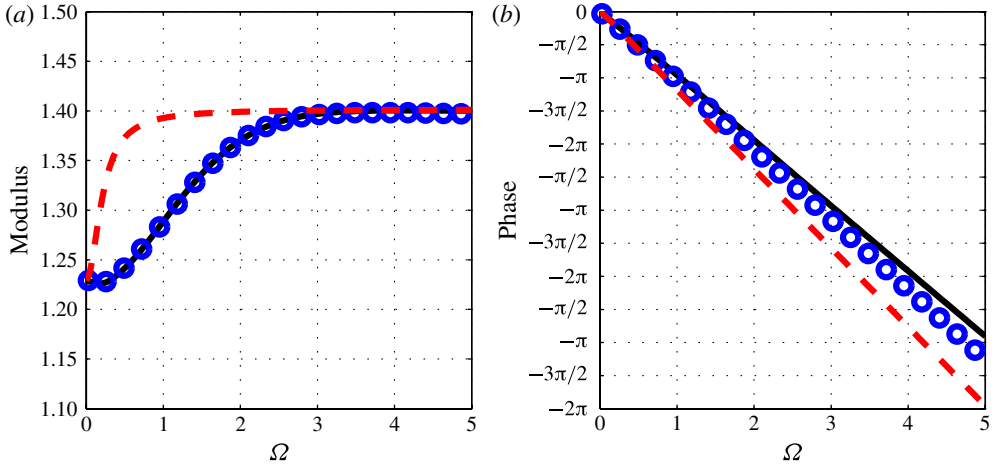


FIGURE 10. (Colour online) Amplitude and phase of the acoustic wave at the outlet w_1^+ generated by an incoming acoustic wave at the inlet w_0^+ . Geometry obtained with (6.2) and solved using the invariants method (—) and numerically (○); linear steady velocity profile (---).

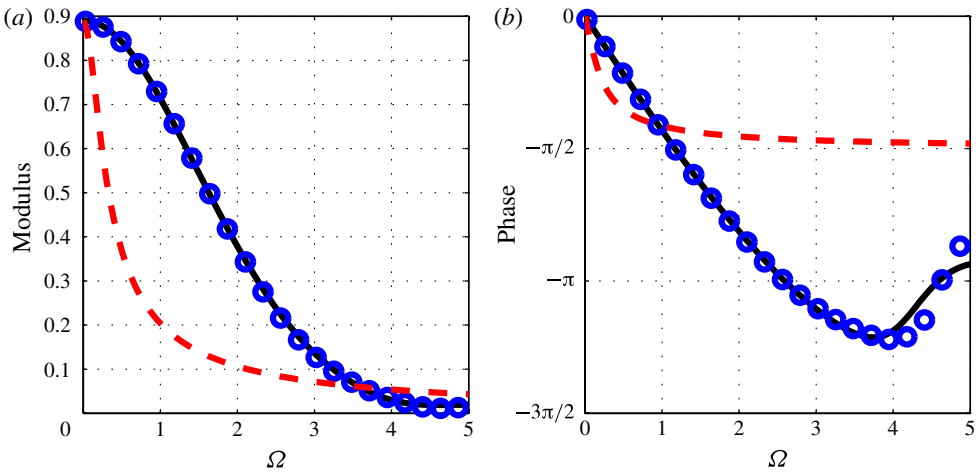


FIGURE 11. (Colour online) Amplitude and phase of the reflected acoustic wave at the inlet w_0^- generated by an incoming acoustic wave at the inlet w_0^+ . Geometry obtained with (6.2) and solved using the invariants method (—) and numerically (○); linear steady velocity profile (---).

the geometry and Mach number distribution are significantly different from the linear velocity profile one.

Using the nozzle geometries shown in figure 9, the transfer functions of an incident acoustic wave are calculated. The subdivision used in the Magnus expansion to reach $\Omega = 5$ are also shown. Figure 10 shows the downstream-propagating acoustic wave at the outlet generated by an acoustic wave at the inlet, and figure 11 shows the reflection coefficient of the nozzle, calculated both for the linear nozzle using the hypergeometric solution of the Appendix and for the realistic nozzle of (6.2) using

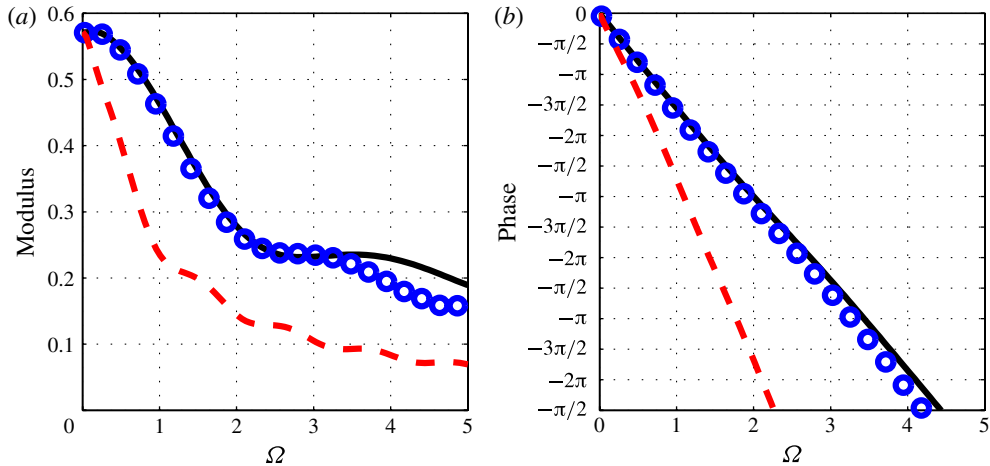


FIGURE 12. (Colour online) Amplitude and phase of the acoustic wave at the outlet w_1^+ generated by an incoming entropy wave at the inlet w_0^s . Geometry obtained with (6.2) and solved using the invariants method (—) and numerically (○); linear steady velocity profile (---).

the invariants method and the Magnus expansion. As expected, at zero frequency there is no difference between the two nozzles, but both the modulus and phase of the transfer functions present large differences when considering non-zero frequencies even if the inlet and the outlet Mach numbers are the same. This shows that, while for the compact case the transfer functions depend only on the inlet and the outlet Mach numbers, the non-compact solution depends strongly on the evolution of the mean flow through the nozzle and therefore on the nozzle geometry.

The transfer functions of the realistic nozzle geometry calculated with the Magnus expansion are also compared with a numerical solver (Silva 2010; Giauque, Huet & Clero 2012), solving the linearized Euler equations in the frequency domain with a second-order centred spatial scheme. The discretization is such as to have at least 100 points per acoustic wavelength for $\Omega = 5$ at the inlet. It can be seen that the analytical method agrees with the numerical simulations, and some discrepancies can only be found at high values of the reduced frequency. Figure 12 shows the indirect noise generated by an entropy wave in the same nozzle. Again, it should be noted that the transfer function depends on the nozzle geometry (and not only on the inlet/outlet Mach number) for non-zero frequencies. The transfer functions of the realistic nozzle geometry are again compared with numerical simulations, showing a fair agreement up to $\Omega = 3$, where the numerical scheme starts to present some dispersion of the entropy wave. The same numerical discretization as for the acoustic transfer function has been used, and therefore about 30 points per entropy wavelength are used at $\Omega = 5$. The computational cost of solving the linearized Euler equations numerically is at least 100 times larger than computing the Magnus expansion of §4, and for a fixed numerical resolution (number of points per entropy wavelength) this difference increases as the minimum Mach number of the nozzle decreases.

6.2. Comparison with experimental measurements

The analytical method proposed in §4 eliminates the compact hypothesis used previously to calculate the transfer functions of the nozzle, but is still based on strong

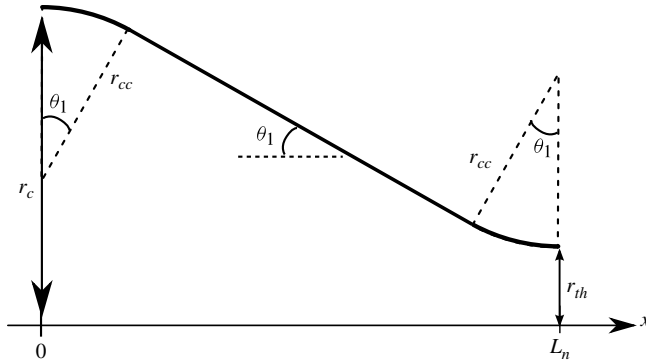


FIGURE 13. Axisymmetric nozzle geometry of Bell *et al.* (1973).

assumptions. These simplifications, such as considering a steady, inviscid main flow, neglecting boundary layers or considering a one-dimensional flow inside the nozzle, can only be verified when compared either with fully turbulent three-dimensional high-fidelity numerical simulations, in which every length scale of the flow is considered, or with experimental data in real configurations. Bell *et al.* (1973) and Zinn *et al.* (1973) developed an experiment to measure the admittance of several rocket engine nozzle geometries, showing the influence of the nozzle geometry on the admittance at non-zero frequencies. This experiment is used in this section to validate the invariants method.

The axisymmetric nozzles considered by Bell *et al.* (1973) are shown in figure 13, where the contour of the nozzle, $r(x)$, is plotted. They are made up of three sections: first, a circular arc of radius r_{cc} starting at the inlet and turned an angle θ_1 ; this arc joins a conical section with the same half-angle, connecting with the third part, a circular arc of the same radius turned an angle of θ_1 . Knowing that the nozzles are all choked, the geometry of the converging section is fully defined with the inlet Mach number and the two geometrical parameters θ_1 and r_{cc}/r_c (the ratio of curvature of the inlet and outlet arcs over the nozzle inlet radius). As the nozzles are choked, the diverging section is not detailed, as it has no effect on the reflecting properties at the inlet (waves do not propagate upstream in the supersonic part).

To compare against experimental data, the admittance (Y) will be used, which is defined as the inverse of the impedance of the nozzle (Z), and can be calculated as

$$Y = \frac{1}{Z} = \rho c \frac{u'}{p'} \Big|_0 = \frac{Mv}{\varphi} \Big|_0. \quad (6.3)$$

To calculate the admittance using the analytical method, the mean flow is obtained by solving (6.1), and therefore viscous effects, boundary layers and two- and/or three-dimensional effects are neglected. The invariants equation is solved setting all incoming waves to zero except the incoming acoustic wave $w_0^+ = 1$. The reflected wave w_0^- is obtained in this way and, using (2.7), the admittance can be calculated as

$$Y = \frac{w_0^+ - w_0^-}{w_0^+ + w_0^-} = \frac{1 - R_0}{1 + R_0}, \quad (6.4)$$

where $R_0 = w_0^-/w_0^+$ is the reflection coefficient. Results will be plotted as a function of the non-dimensional frequency $S = 2\pi fr_c/c_0$ as done by Bell *et al.* (1973), where

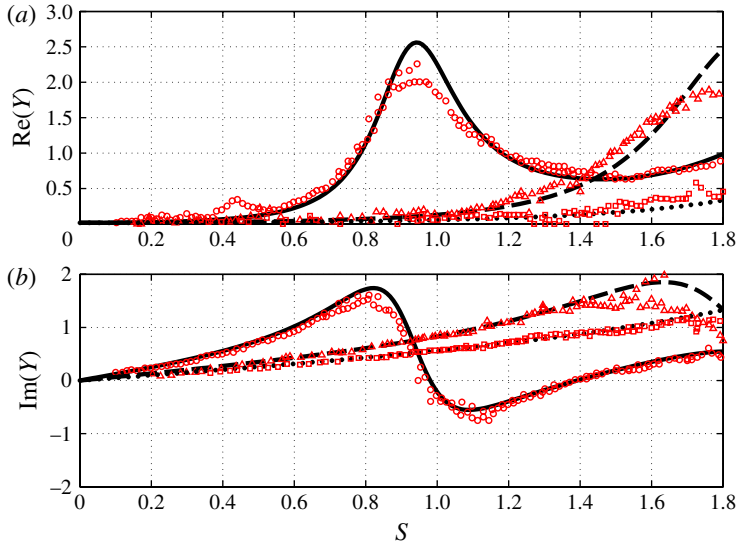


FIGURE 14. (Colour online) Real and imaginary parts of the acoustic admittance Y of three different choked nozzles; $M_0 = 0.08$, $r_{cc}/r_c = 0.44$. For $\theta_1 = 15$: analytical (—), experiments (\circ). For $\theta_1 = 30$: analytical (— —), experiments (\triangle). For $\theta_1 = 45$: analytical (\cdots), experiments (\square).

the angular frequency ($2\pi f$), the nozzle inlet radius (r_c) and sound speed (c_0) are used. This reduced frequency can be easily related to the one used previously in this paper ($S = 2\pi\Omega r_c/L_n$) but S will be used in this section as done by Bell *et al.* (1973) to compare with their results.

Out of all the cases studied by Bell *et al.* (1973), three will be considered here, corresponding to an inlet Mach number of 0.08, a radius ratio $r_{cc}/r_c = 0.44$ and three half-angles, $\theta_1 = 15, 30$ and 45° . Figure 14 shows the admittance of the three nozzles computed with the analytical method of §4 compared to the experimental values. Bell *et al.* (1973) compared their results with Crocco's theory (Crocco & Sirignano 1967) with which, under similar hypotheses as used for the invariants theory, the nozzle admittance was obtained by integrating numerically a nonlinear Riccati equation. These numerical results perfectly match with the invariants solution and are not shown here but can be found in figure 4 of Bell *et al.* (1973). In figure 14 the analytical solution obtained with the flow invariants using the Magnus expansion compares well with the experimental data within the experimental error and the limitations of the invariants theory. This shows that the invariants theory can be used to compute reflection coefficients (impedances or admittances) of rocket engine nozzles or gas-turbine nozzles for combustion instability studies. Results also illustrate that the reflecting properties of one-dimensional nozzles strongly depend on the geometry of the converging section when considering non-zero frequencies, showing the interest of an analytical method able to solve the propagation of waves through any nozzle geometry, even if strong assumptions are still being made.

6.3. Comparison with the 'equivalent nozzle length' method for choked nozzles

The method of Stow *et al.* (2002) in which the phase of the reflection coefficient is corrected through an equivalent nozzle length is here compared with the invariant

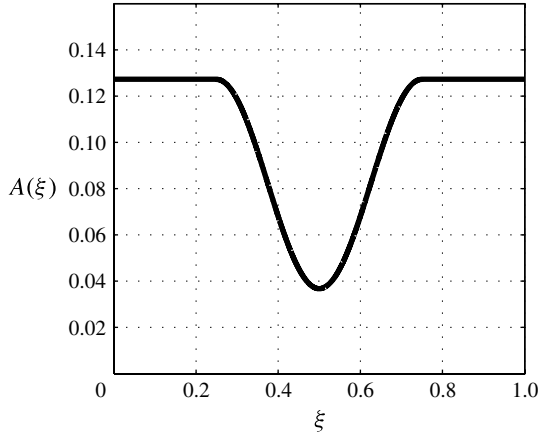


FIGURE 15. Plot of $A(\xi)$ of the nozzle of Stow *et al.* (2002).

method. The phase correction of the inlet reflection coefficient is written as

$$\left[\frac{w_0^-}{w_0^+} \right] = \left[\frac{w_0^-}{w_0^+} \right]_{MC} \exp[-i(k^+ + k^-)l\Omega], \quad (6.5)$$

where the subscript $[\]_{MC}$ represents the transfer function computed through the compact nozzle hypothesis (as seen in table 2). For the reflection coefficient of a choked nozzle it reads

$$\left[\frac{w_0^-}{w_0^+} \right]_{MC} = \frac{1 - \frac{1}{2}(\gamma - 1)M_0}{1 + \frac{1}{2}(\gamma - 1)M_0}. \quad (6.6)$$

In the above, $k^+ = 2\pi/(M_0 + 1)$ and $k^- = 2\pi/(M_0 - 1)$ are the dimensionless wavenumbers, and the equivalent nozzle length l is computed using the asymptotic expansion of the linearized Euler equations up to first order and considering a low Mach number at the inlet (for more details see Stow *et al.* (2002)). It reads

$$l = \int_0^{\xi_*} \frac{\bar{u}(0)}{\bar{u}(\xi)} d\xi. \quad (6.7)$$

This correction is valid for choked nozzles and in the case of small inlet Mach numbers. As seen in (6.5), the correction affects the phase prediction only, leaving the modulus of the solution constant and equal to the compact prediction.

The geometry considered for this analysis is the one used by Stow *et al.* (2002) for their study (see figure 15), with a choked flow. Figure 16 shows the reflection coefficient of the choked nozzle obtained using both methods. It is shown that the effective nozzle length successfully corrects the phase of the reflection coefficient. The invariants method, however, corrects both the phase and the modulus of the transfer functions. The numerical results of Stow *et al.* (2002) are also reproduced in the figure for the sake of comparison.

The equivalent nozzle length method was extended by Goh & Morgans (2011a) to compute the phase of the transmission coefficients for the acoustic and the entropy waves. This method is based on the combination of several equivalent lengths through the convergent and the divergent sections to obtain the correct phase prediction of the transfer functions of the nozzle in a similar way as the reflection coefficient (for

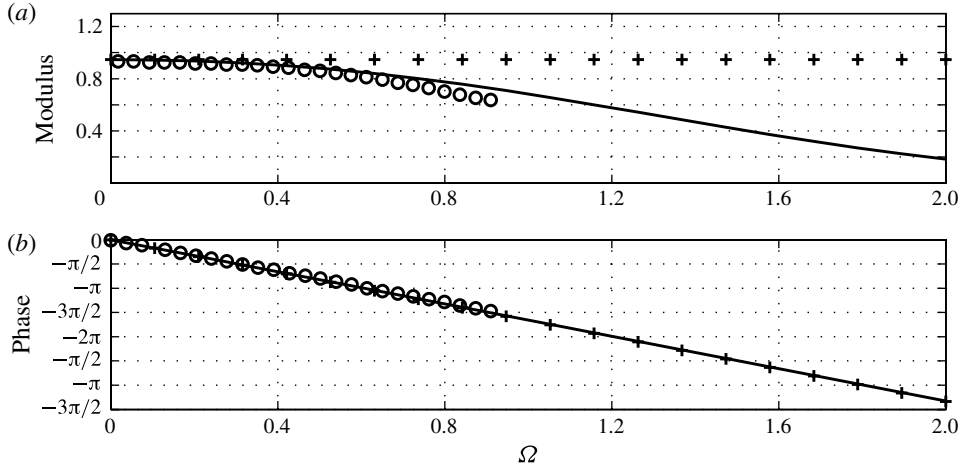


FIGURE 16. Amplitude and phase of the reflected acoustic wave at the inlet of the nozzle (w_0^- due to w_0^+). Stow's equivalent length method (+), Stow's numerical results (O), and invariants method (—).

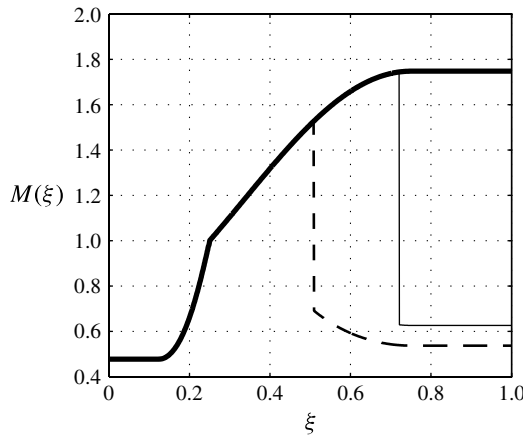


FIGURE 17. Plot of $M(\xi)$ of the nozzle used in Goh & Morgans (2011a) for three flow configurations: choked isentropic (thick line), choked with a shock wave at the nozzle exit (thin line), and choked with a shock wave in the divergent (dashed line).

more details see Goh & Morgans (2011a)). Their results are compared here with the invariants method for three flow configurations: choked, choked with a shock wave at the exit, and choked with a shock wave in the divergent section. For simplicity, the geometry used is the same as in Goh & Morgans (2011a), where the steady Mach number has been calculated analytically using the steady quasi-one-dimensional equations and is plotted in figure 17 for the three flow configurations studied hereafter.

Figures 18 and 19 show the acoustic wave at the outlet of the nozzle generated by an acoustic and an entropy perturbation at the inlet for the choked case. The transfer function is computed using three different methods: the compact hypothesis of Marble & Candel (1977), the first-order correction of the phase (Goh & Morgans 2011a) and

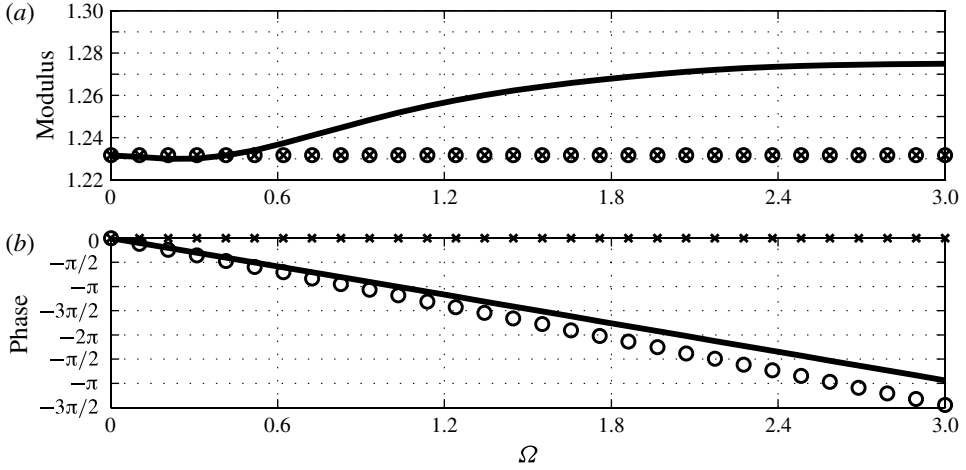


FIGURE 18. Amplitude and phase of the transmitted acoustic wave generated by an acoustic perturbation at the inlet for a choked nozzle. Equivalent nozzle length method (\circ), Marble and Candel method (\times), and invariants method (—).

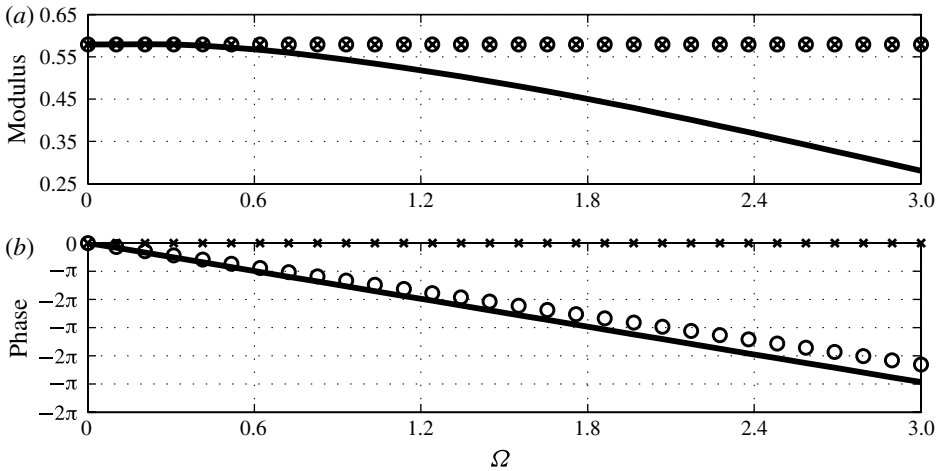


FIGURE 19. Amplitude and phase of the transmitted acoustic wave generated by an entropy perturbation at the inlet for a choked nozzle. Equivalent nozzle length method (\circ), Marble and Candel method (\times), and invariants method (—).

the invariants method presented previously. Results show that the equivalent length method of Goh gives a fair correction of the phase of the transmission coefficient for small frequencies only. The modulus of the transmission coefficient, however, is also found to vary with the frequency of the inlet perturbation due to the non-compact propagation of waves through the nozzle. This effect represents a significant difference at non-zero frequencies, which cannot be corrected with the effective nozzle length method, showing the advantage of a complete analytical solution of the linearized Euler equations up to any order in Ω .

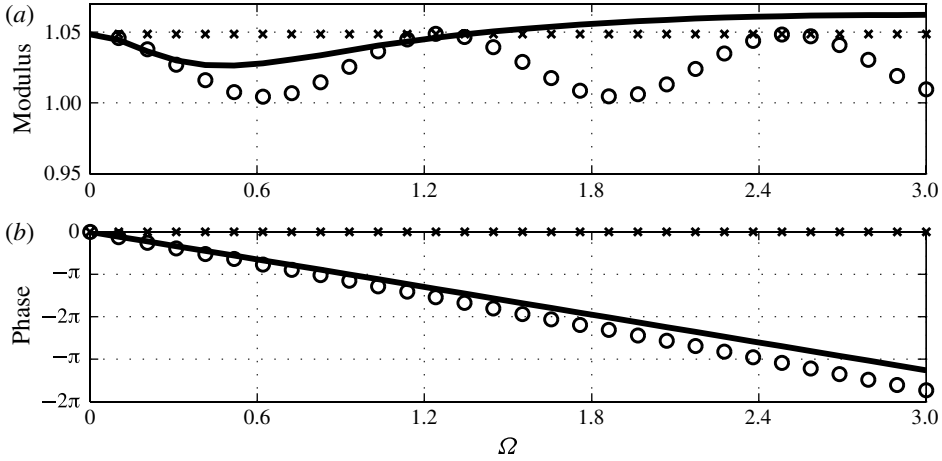


FIGURE 20. Amplitude and phase of the transmitted acoustic wave generated by an acoustic perturbation at the inlet for the choked case with a shock wave at the end of the nozzle. Equivalent nozzle length method (O), Marble and Candel method (x), and invariants method (—).

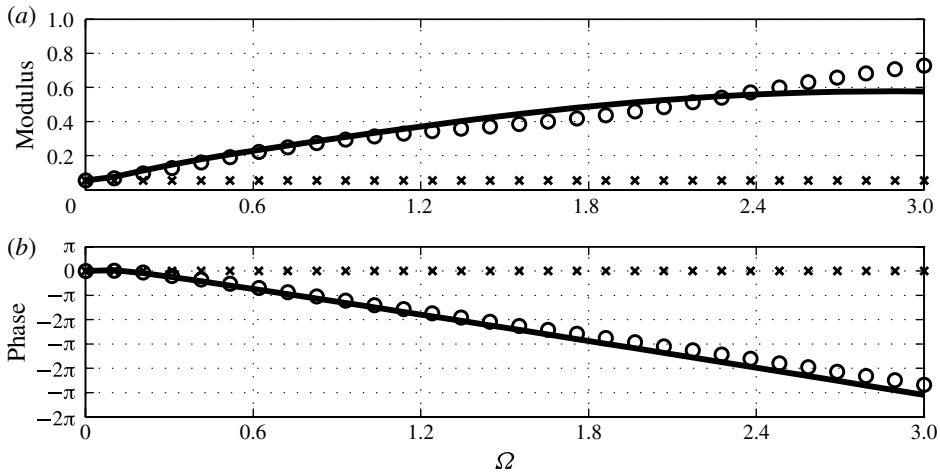


FIGURE 21. Amplitude and phase of the transmitted acoustic wave generated by an entropy perturbation at the inlet for the choked case with a shock wave at the end of the nozzle. Equivalent nozzle length method (O), Marble and Candel method (x), and invariants method (—).

When considering a flow with a shock wave inside the nozzle, the interaction of the acoustic waves with the shock has to be considered, as seen in § 5.3. First of all, the case of a shock wave at the outlet of the nozzle is considered, as done in Goh & Morgans (2011a). In this case, the terms $dM_a/d\xi$ of (5.17) are zero and the transfer functions through the shock wave therefore become frequency-independent. Figures 20 and 21 show the acoustic wave generated at the outlet by an incoming acoustic and entropy wave at the inlet, respectively, calculated using Marble and Candel’s compact solution for the propagation of waves through a nozzle with a shock wave, the equivalent length method of Goh and the invariants method. Both corrective methods

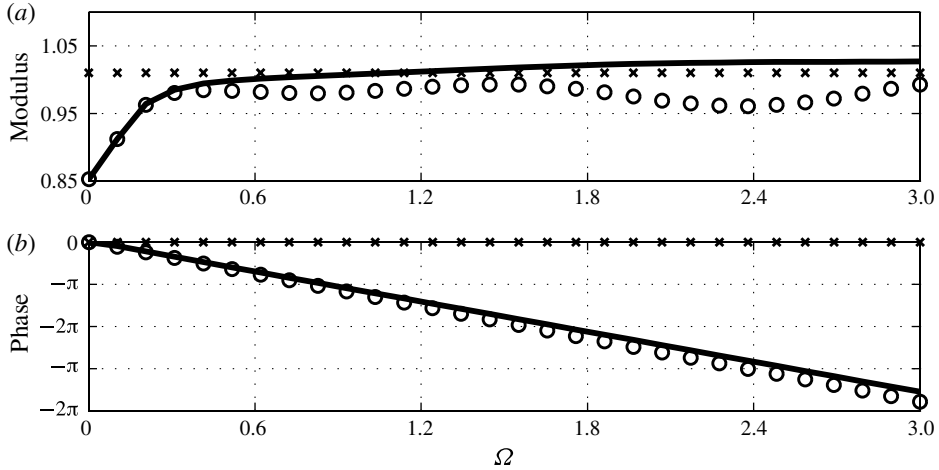


FIGURE 22. Amplitude and phase of the transmitted acoustic wave generated by an acoustic perturbation at the inlet for the choked case with a shock wave. Equivalent nozzle length method (\circ), Marble and Candel method (\times), and invariants method (—).

again show a good agreement for low frequencies, although the first-order correction of the phase through the equivalent nozzle length fails to correctly predict the modulus of the transfer functions at higher frequencies.

The study of the stability of shock waves in a nozzle shows that they are stable only when located in the diverging region of the nozzle. This is why the study of the interaction of acoustic waves with the shock wave should be done when it is located in the divergent section. The shock wave will therefore fluctuate in a region of the nozzle where mean density, pressure, Mach number and velocity gradients exist. Taking into account these mean flow gradients, the solution explained in § 5.3 is obtained. In this case the transfer functions of the acoustic and entropy waves through the shock wave are frequency-dependent regardless of the compactness of the nozzle. This is caused by the frequency dependence of the acoustic transfer functions through a shock wave, as seen in table 3. Figures 22 and 23 show the acoustic wave at the outlet of the nozzle generated by an acoustic and an entropy wave at the inlet, respectively, calculated with Marble and Candel's method, the equivalent nozzle length method of Goh and Morgans and the invariants method. Results show a good agreement for low frequencies between the invariants method and the equivalent length method, where the propagation of waves through the nozzle can be considered compact and therefore the frequency dependence of the solution is driven by the transfer functions of the shock wave (table 3). At larger frequencies, however, discrepancies are found caused by the variation of the modulus of the transfer functions of the nozzle upstream and downstream of the shock wave, which Goh and Morgans calculate using the compact nozzle assumption. It should be noted that Marble and Candel's solution shown in figures 22 and 23 does not consider the mean Mach number gradient in (5.11)–(5.13), and therefore is constant with frequency and does not agree with the solutions obtained in § 5.3.

6.4. Study of subsonic nozzles

The solution of the LEEs using the invariants and the Magnus expansion proposed in § 4 can also be used to solve subsonic nozzles of any considered geometry. The nozzle

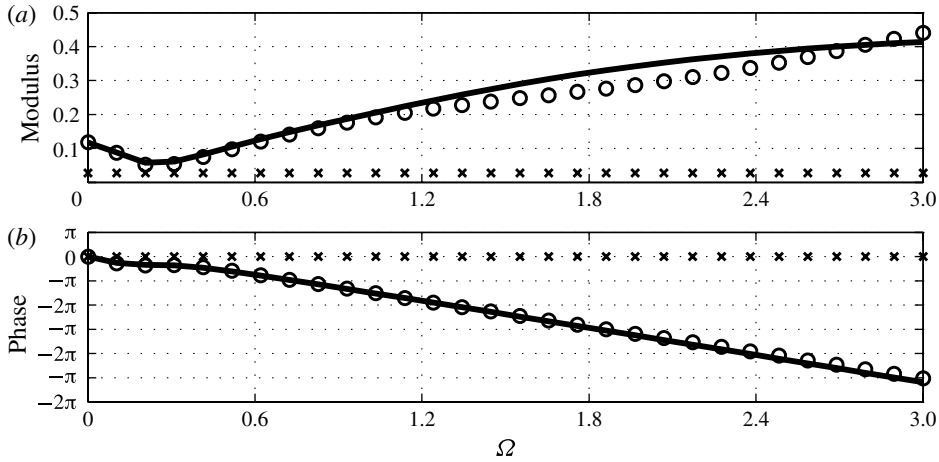


FIGURE 23. Amplitude and phase of the transmitted acoustic wave generated by an entropy perturbation at the inlet for the choked case with a shock wave. Equivalent nozzle length method (\circ), Marble and Candel method (\times), and invariants method (—).

	Inlet Mach number (M_0)	Throat Mach number (M_T)	Outlet Mach number (M_1)
Case 1	0.0305	0.6	0.0171
Case 2	0.0331	0.7	0.0186
Case 3	0.0349	0.8	0.0196

TABLE 4. Mach numbers in the EWG nozzle for the three mean flow configurations considered.

analysed here is the one used for the entropy wave generator (EWG) experiment. This experiment, performed by Bake *et al.* (2009), studied the indirect noise generated by a convected entropy wave through a nozzle. The subsonic response of the nozzle is here studied as an example for several Mach number profiles as seen in figure 24 and in table 4. To do so, a non-reflecting boundary condition is imposed both at the inlet and at the outlet as we are interested only in the transfer functions. Figure 25 shows the acoustic transmitted and reflected waves generated by a unitary entropy wave at the inlet for several throat Mach numbers. The result shows that the response of the nozzle at non-zero frequencies is significantly different from the solution obtained at $\Omega = 0$. For instance, at $\Omega = 0.1$ the transmitted wave is 40 times larger than the one predicted by the compact theory, and it keeps on increasing with frequency. A similar response is found in the case of the reflected acoustic wave. The compact analysis is therefore limited to very low frequencies in the case of converging–diverging nozzles. The increase of indirect noise generated by the nozzle at non-zero frequencies is caused by the strong acceleration and deceleration of the mean flow in the nozzle throat. This acceleration and deceleration has no effect at zero frequencies, as the indirect noise generated by the converging section is cancelled out by the one generated in the diverging region. This occurs because the indirect noise is generated by the mean velocity gradient of the nozzle, which is positive in the convergent section

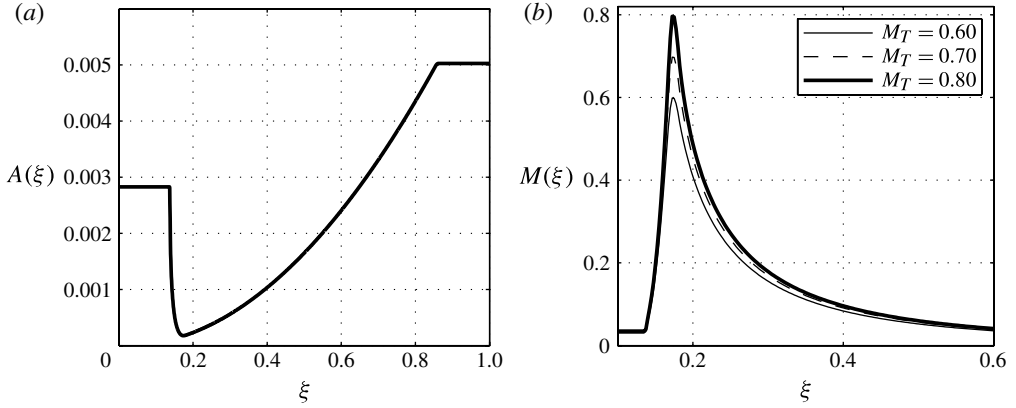


FIGURE 24. Section of the EWG nozzle, and three Mach number profiles, corresponding to three different throat Mach numbers.

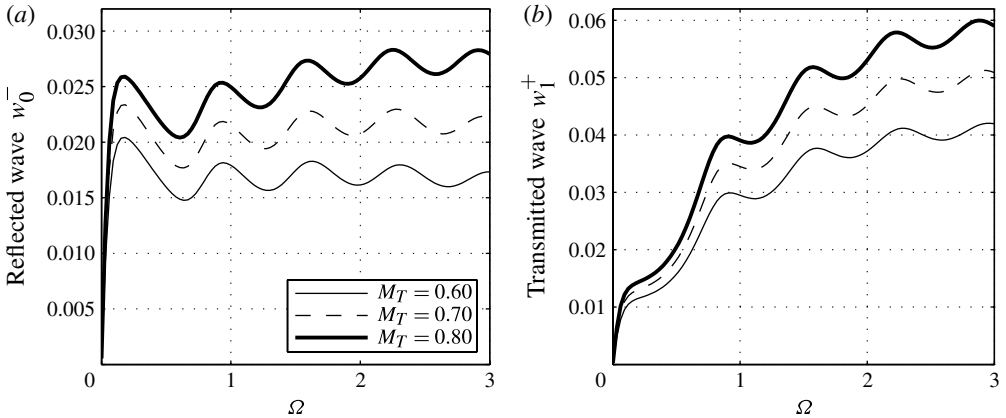


FIGURE 25. Amplitude of the transmitted and reflected acoustic waves generated by an entropy wave in the EWG nozzle for different throat Mach numbers calculated using the invariants.

and negative in the divergent section for subsonic nozzles. At non-zero frequencies, however, the acoustic waves are not perfectly cancelled out due to the phase-shift linked to the different propagation speeds of acoustic and entropy waves inside the nozzle. For this reason indirect noise increases drastically at non-zero frequencies. This does not occur in choked nozzles as shown in figure 5 as the mean velocity gradient is always positive.

Figure 25 also shows that, when considering the compact nozzle solution, the response of the nozzle is almost unaltered when changing the Mach number profile. For zero frequencies, the transfer function is only dependent on the inlet and outlet Mach numbers (see table 1), which are only slightly changed for the three cases studied here. However, for increasing frequencies, the Mach number profile is shown to have a strong influence on the entropy transfer functions. The entropy transfer function depends on the complete Mach number profile and, in the case of the converging–diverging nozzle studied here, the small variations of Mach number at

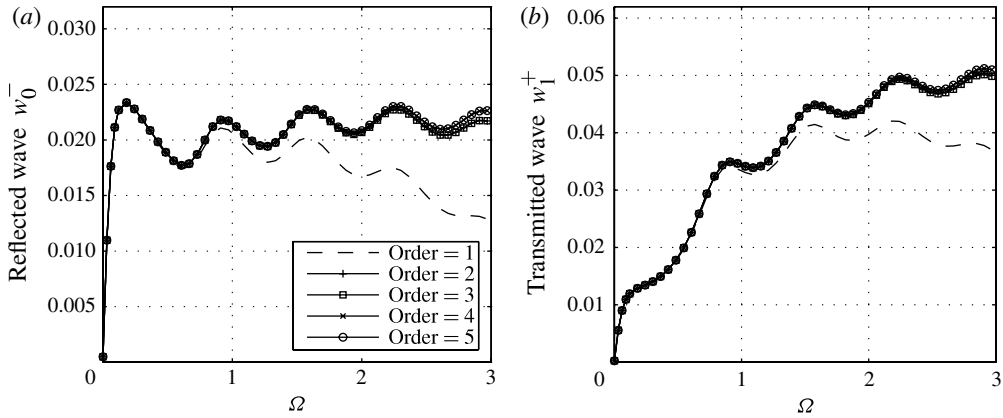


FIGURE 26. Amplitude of the transmitted and reflected acoustic waves generated by an entropy wave in the EWG nozzle for $M_T = 0.7$ calculated using the invariants at different orders of the Magnus expansion.

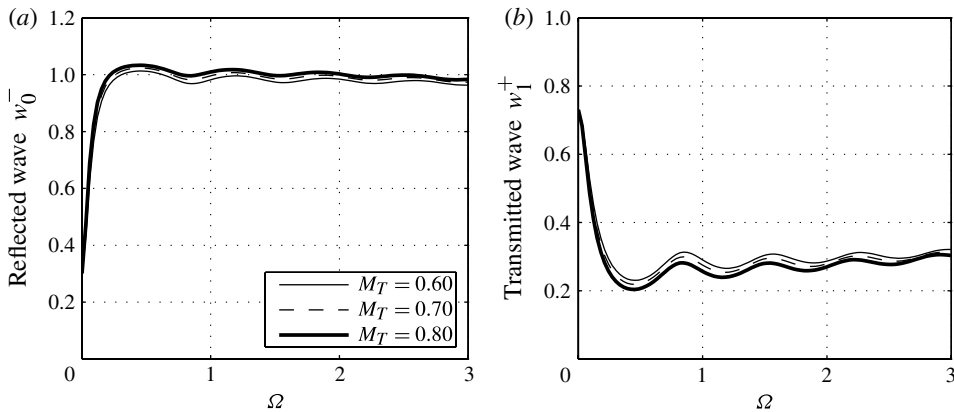


FIGURE 27. Amplitude of the acoustic transmission and reflection coefficients of the EWG nozzle calculated using the invariants.

the inlet induce large variations of the throat Mach number as seen in table 4, which will in turn strongly modify the transfer functions at non-zero frequencies.

Figure 26 shows the same plot as in figure 25 for the case $M_T = 0.7$ only calculated using the Magnus expansion at different orders to show the convergence of the method. It can be seen that an order four or five is enough to calculate the modulus of the entropy transfer functions.

The EWG nozzle geometry can be used to study the response of a subsonic nozzle to acoustic perturbations. In figure 27 the reflection and transmission coefficients similarly show that the solution for non-zero frequencies strongly differs from the compact solution at $\Omega = 0$. The evolution of the reflection coefficient of this subsonic nozzle is the inverse of the one observed in the choked nozzle (figure 7): in the choked case the reflection coefficient at $\Omega = 0$ is ~ 0.9 and tends to zero when Ω increases,

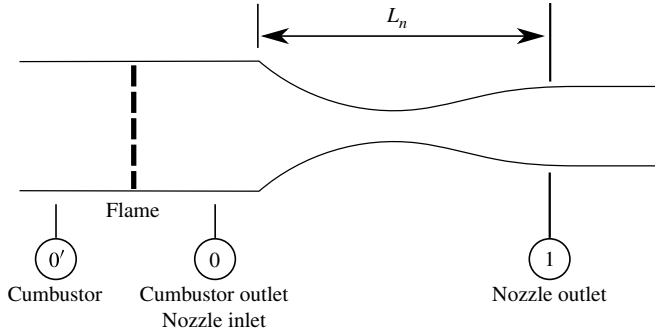


FIGURE 28. Simplified model of a combustor used by Leyko *et al.* (2009).

while for the subsonic case the reflection coefficient is small at $\Omega = 0$ and increases thereafter towards one.

In the case of acoustic disturbances entering the nozzle, the influence of the Mach number profile through the nozzle is very limited. Figure 27 shows that the three cases studied are almost identical.

6.5. Parametric study on direct and indirect combustion noise

The analytical solution of the LEEs through the invariants method can be used to perform a parametric study of combustion noise at the outlet of a combustion chamber, which is critical for a proper estimate of transmission losses through turbine stages and could explain the observed aft spectra of small turbo-engines and helicopter turbo-shaft engines. When a turbulent confined flame fluctuates, it generates both entropy and acoustic waves. The propagation of these waves generates two types of noise: direct noise, produced by the acoustic waves that propagate through the turbine stages and reach the outlet, and indirect noise, generated inside the turbo-machinery by the acceleration of entropy waves generated during combustion. The relative importance of indirect noise is therefore linked to the propagation of waves through a non-uniform flow. Leyko *et al.* (2009) compared the direct and indirect combustion noise generated in a model combustor. The analysis performed was based on a simple tube with a one-dimensional cold flame followed by a compact converging–diverging nozzle as illustrated in figure 28. A cold flame is a simplification in which a flame is considered to generate only fluctuating heat release, with no mean value. With this simplification, the mean flows upstream and downstream of the flame are assumed to be equal, as was done by Leyko *et al.* (2009). Using this simple model, the ratio of indirect to direct noise generated by a fluctuating heat release was estimated for different Mach numbers using the compact nozzle hypothesis. To solve the compact cold flame Leyko *et al.* (2009) used the compact equations (2.1)–(2.3) written between the inlet and the outlet of the cold flame, with a fluctuating heat source term \dot{Q}' in both the energy and the entropy equations:

$$(\dot{m}')_{0'} = (\dot{m}')_0, \quad (6.8)$$

$$(c_p \dot{m} T'_t)_{0'} + \dot{Q}' = (c_p \dot{m} T'_t)_0, \quad (6.9)$$

$$(\dot{m} s')_{0'} + \frac{\dot{Q}'}{T} = (\dot{m} s')_0. \quad (6.10)$$

Defining the dimensionless fluctuating heat release as $q' = \dot{Q}' / (\dot{m} c_p T)$ and knowing that $M_{0'} = M_0$ for the cold flame, the equations can be written using the primitive variables:

$$(\varphi + \nu - \sigma)_{0'} = (\varphi + \nu - \sigma)_0, \quad (6.11)$$

$$[(\gamma - 1)M^2\nu + (\gamma - 1)\varphi + \sigma]_{0'} + q' = [(\gamma - 1)M^2\nu + (\gamma - 1)\varphi + \sigma]_0, \quad (6.12)$$

$$(\sigma)_{0'} + q' = (\sigma)_0. \quad (6.13)$$

Using the waves definition (2.7) and imposing no incoming waves ($w_{0'}^+ = 0$, $w_{0'}^s = 0$, $w_0^- = 0$), the outgoing entropy and acoustic waves generated by the heat release fluctuation q' read

$$w_0^s = q', \quad w_0^+ = \frac{M_0}{1 + M_0} q' \quad \text{and} \quad w_{0'}^- = \frac{M_0}{1 - M_0} q'. \quad (6.14)$$

The ratio of indirect to direct combustion noise, η , is defined as the ratio of the acoustic waves generated at the outlet of the nozzle by the entropy waves (indirect noise) to the acoustic waves at the outlet generated by the propagation of the acoustic waves produced by the fluctuating heat release. It follows that

$$\eta = \underbrace{\frac{w_1^+}{w_0^s}}_{\text{entropy TF}} \times \underbrace{\frac{w_0^s}{w_0^+}}_{\text{wave ratio}} \times \underbrace{\left[\frac{w_1^+}{w_0^+} \right]^{-1}}_{\text{acoustic TF}}, \quad (6.15)$$

where the ‘wave ratio’ term is obtained from (6.14). The first term is the entropy transfer function of the nozzle, which gives the acoustic wave generated by a unitary entropy wave. Similarly, the third term is the acoustic transfer function. Leyko *et al.* (2009) calculated both transfer functions using the compact nozzle hypothesis (tables 1 and 2) obtaining an analytical expression

$$\eta = \frac{1}{M_0} \frac{(M_1 - M_0)(M_1 + M_0)}{2 \left(1 + \frac{1}{2}(\gamma - 1)M_1^2\right)} \quad \text{for subsonic nozzles} \quad (6.16)$$

$$\eta = \frac{1 + M_0}{M_0} \frac{(M_1 - M_0)}{2 \left(1 + \frac{1}{2}(\gamma - 1)M_1\right)} \quad \text{for the choked case.} \quad (6.17)$$

Using this compact solution, Leyko *et al.* (2009) evaluated the ratio of indirect to direct noise for different inlet and outlet Mach numbers. The invariants method is here used to obtain the indirect to direct noise ratio as a function of the frequency of the fluctuating heat release. To do so, the nozzle geometry of (6.2) is considered for the choked cases. In the subsonic case only a converging section is used, for simplicity. The invariants are solved for different inlet and outlet Mach numbers to calculate the indirect to direct noise ratio η for reduced frequencies Ω from 0 to 2.5. In total 2500 different nozzle geometries are solved at six frequencies, the complete calculation taking less than 2.5 h on a single CPU (2.66 GHz). Figure 29 shows the noise ratio as a function of the inlet and the outlet Mach numbers for several frequencies. The results show a perfect agreement between the compact solution and the invariants one calculated at $\Omega = 0$. For larger frequencies, the indirect to direct noise ratio decreases as Ω increases, which means indirect noise is only significant at low frequencies and could be neglected at high frequencies.

The results can be analysed through previous results obtained in § 6.1. Figure 5 shows that, for choked nozzles, the indirect noise generated by a unitary entropy wave

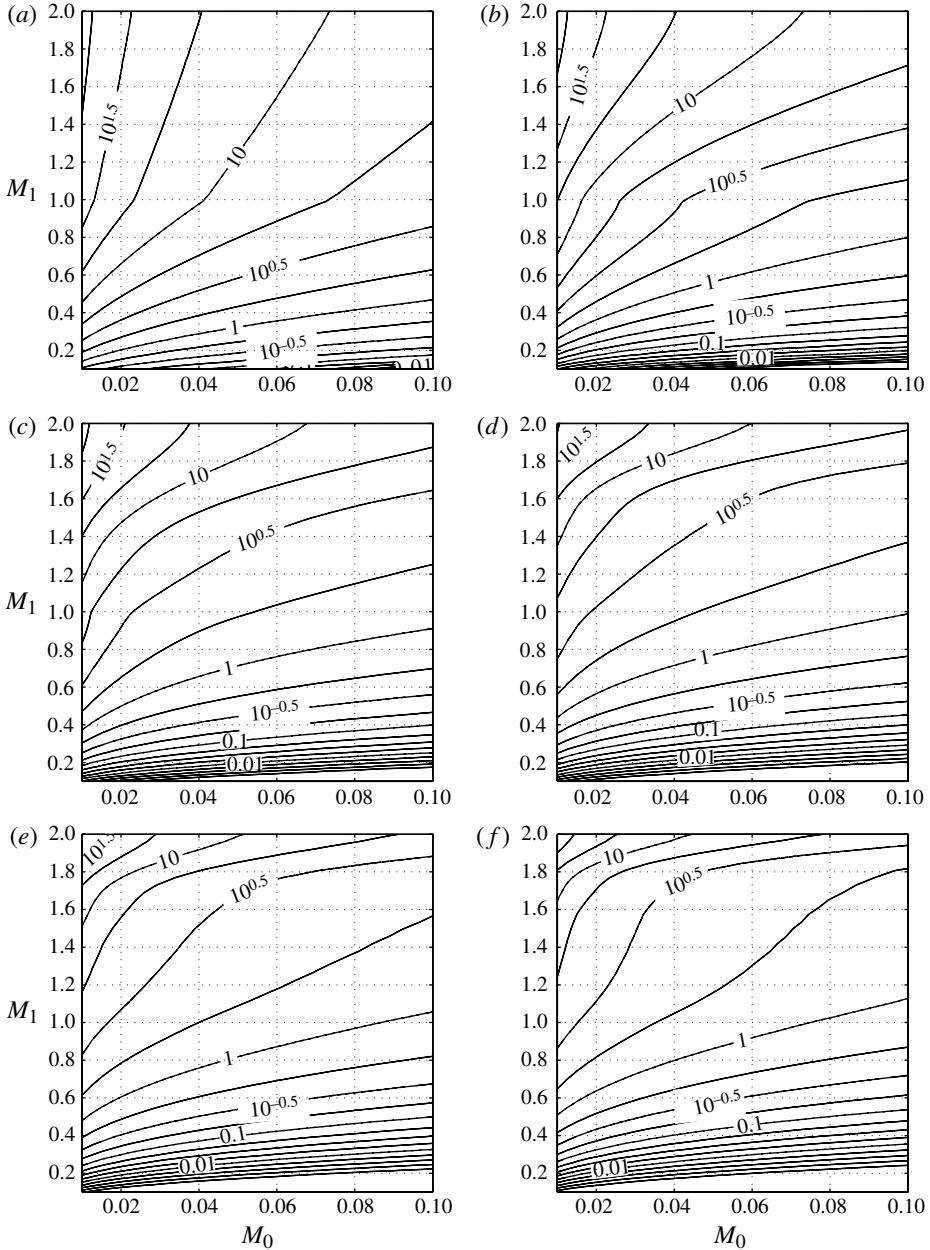


FIGURE 29. Indirect to direct noise ratio η calculated using the invariant method as a function of the inlet and the outlet Mach numbers of the nozzle, M_0 and M_1 , for different frequencies: (a) η at $\Omega = 0$; (b) η at $\Omega = 0.5$; (c) η at $\Omega = 1$; (d) η at $\Omega = 1.5$; (e) η at $\Omega = 2$; (f) η at $\Omega = 2.5$.

at the inlet decreases with increasing frequency. On the other hand, the direct noise generated by an acoustic wave at the inlet (shown in figure 10 for the same nozzle) increases slightly with Ω and then remains constant. The effect of both terms will add up to give an indirect to direct noise ratio η that will decrease with Ω . In the

subsonic region of figure 29 it can also be seen that the indirect to direct noise ratio decreases with increasing frequency. However, this result can be shown to depend on the nozzle geometry considered. As previously stated, a converging geometry has been used to perform the parametric study. Section 6.4 showed the case of a subsonic converging–diverging nozzle, with low inlet and outlet Mach numbers but a strong acceleration of the flow at the nozzle throat. Results in figures 25 and 27 show that indirect noise increases with frequency and that direct noise decreases, giving therefore an indirect to direct noise ratio that will strongly increase with frequency for the considered nozzle geometry. This shows the importance of an analytical solution valid for any nozzle geometry and any flow condition.

7. Conclusion

An analytical solution for the one-dimensional linearized Euler equations has been found, combining the invariants equations with the Magnus solution of a linear system of differential equations with varying coefficients. Boundary conditions have been applied for both subsonic and choked cases. This solution has been successfully validated with the analytical solution found by Marble & Candel (1977) for the case of a nozzle with a linear steady velocity profile. The analytical method through the flow invariants extends the solution of both Stow *et al.* (2002) and Goh & Morgans (2011a), predicting both the phase and the modulus of the transfer functions as a function of frequency in any flow configuration with any nozzle geometry, and generalizing the solution up to any order in the asymptotic expansion. The present solution also removes the inherent assumption of a piecewise-linear approximation of the velocity profile in the nozzle assumed by Moase *et al.* (2007) in their generalization of the hypergeometric solution of Marble & Candel (1977). It can deal with any arbitrary velocity profile in C^0 , or equivalently any nozzle geometry and back-pressure. Therefore, the present method based on invariants and the Magnus expansion extends and unifies all existing asymptotic or piecewise solutions to the quasi-one-dimensional linearized Euler equations, and prevents any convergence, dispersion and dissipation issues and computational cost associated with numerical methods.

Results show that the transfer functions of choked nozzles vary strongly with the frequency of the perturbation. This strong variation affects both the transmission and the reflection coefficients of entropy and acoustic waves, and should be taken into account to correctly predict combustion noise and thermoacoustic instabilities.

The linear steady velocity nozzle profile has also been compared with more realistic nozzles, where the geometry is given through realistic design constraints such as preventing flow separation in the diverging region. This comparison showed that for non-zero frequencies the transfer functions are dependent on the considered geometry, and differ from one nozzle to another even if the inlet and outlet Mach numbers are equal. This demonstrates the interest of a general analytical solution in which any nozzle geometry can be solved in any flow configuration.

The subsonic flow has also been investigated using the invariants method. Results showed that, for the converging–diverging subsonic nozzle used in the EWG experiment, the acoustic waves generated by entropy waves (indirect noise) strongly depend on the frequency of the perturbation. A similar conclusion was drawn when studying the acoustic response of the nozzle, showing again that the non-compact effect should be taken into account when studying noise propagation through accelerating and decelerating flows.

The assumptions made when using the one-dimensional linearized Euler equations limit the results to frequencies lower than the first cut-off frequency and, at the same time, to one-dimensional inviscid flows. The solution has been compared with experimental data of rocket engine nozzles, showing a good agreement, regardless of the assumptions made. This shows that the method can be used to obtain a correct estimate of the reflection coefficient of nozzles, even if the flow details, turbulence and boundary layers are neglected. An improvement of the method could be to consider the boundary-layer displacement thickness to obtain a more realistic mean flow through the nozzle before solving the invariant equations. The comparison with experimental data shows at the same time that the reflecting properties of a choked nozzle strongly depend on the geometry considered at non-zero frequencies and that the invariants method is able to predict this behaviour for both the modulus and the phase of the reflecting properties. This is particularly important for the analysis of combustion instabilities as the reflecting condition of choked nozzles monitors the energy loss through the outlet, and therefore the stability of the mode itself.

A parametric study of indirect to direct noise ratio has been finally performed. This study generalizes the work done by Leyko *et al.* (2009), who made a parametric study of nozzles for the compact case. The non-compact parametric study was carried out, showing that, for the type of geometry considered, the indirect to direct noise ratio as defined by Leyko *et al.* (2009) globally decreased with frequency, and consequently the indirect noise source should prevail only at low frequencies.

Appendix

Marble & Candel (1977) proposed an analytical method to solve the LEEs (3.1)–(3.3) in a nozzle with a linear steady velocity profile. The origin of the x coordinate system is taken where the steady velocity is zero. Using the subscript $(*)$ for quantities taken at the choked section, the dimensionless time and space coordinates can be defined as $\hat{\tau} = tc_*/x_*$ and $\hat{\xi} = (x/x_*)^2 = (u/u_*)^2$ if $x = 0$ is taken where $u = 0$ (even if this point is extrapolated outside the computational domain). Marble & Candel (1977) used these variables to transform (3.1)–(3.3) into

$$\left[\frac{\partial}{\partial \hat{\tau}} + 2\hat{\xi} \frac{\partial}{\partial \hat{\xi}} \right] (\varphi) + 2\hat{\xi} \frac{\partial}{\partial \hat{\xi}} (v) = 0, \quad (\text{A } 1)$$

$$\left[\frac{\partial}{\partial \hat{\tau}} + 2\hat{\xi} \frac{\partial}{\partial \hat{\xi}} \right] (v) + \left[\frac{\gamma - 1}{\hat{\xi}} - \gamma + 1 \right] \hat{\xi} \frac{\partial}{\partial \hat{\xi}} (\varphi) + 2v - (\gamma - 1)\varphi - \sigma = 0, \quad (\text{A } 2)$$

$$\left[\frac{\partial}{\partial \hat{\tau}} + 2\hat{\xi} \frac{\partial}{\partial \hat{\xi}} \right] (\sigma) = 0. \quad (\text{A } 3)$$

Assuming that the disturbances are harmonic, $\varphi = P(\hat{\xi}) \exp(i\hat{\Omega}\hat{\tau})$, $v = U(\hat{\xi}) \exp(i\hat{\Omega}\hat{\tau})$ and $\sigma = \sigma(\hat{\xi}) \exp(i\hat{\Omega}\hat{\tau})$ are used, with $\hat{\Omega} = 2\pi f x_*/c_*$. Equation (A 3) is directly solved, giving

$$\sigma = \sigma_r \left(\frac{\hat{\xi}}{\hat{\xi}_r} \right)^{-i\hat{\Omega}/2}, \quad (\text{A } 4)$$

and this result is combined with (A 1)–(A 2) to obtain a hypergeometric equation for P ,

$$\hat{\xi}(1 - \hat{\xi}) \frac{d^2 P}{d\hat{\xi}^2} - \left[2 + \frac{2i\hat{\Omega}}{\gamma + 1} \right] \hat{\xi} \frac{dP}{d\hat{\xi}} - \frac{i\hat{\Omega}(2 + i\hat{\Omega})}{2(\gamma + 1)} P = -\sigma_r \frac{i\hat{\Omega}}{2(\gamma + 1)} \left(\frac{\hat{\xi}}{\hat{\xi}_r} \right)^{-i\hat{\Omega}/2}, \tag{A 5}$$

where $U(\hat{\xi})$ has been eliminated. Once this equation is solved, $U(\hat{\xi})$ is given by

$$(2 + i\hat{\Omega})U = -(\gamma + 1)(1 - \hat{\xi}) \frac{dP}{d\hat{\xi}} + (\gamma - 1 + i\hat{\Omega})P + \sigma_r \left(\frac{\hat{\xi}}{\hat{\xi}_r} \right)^{-i\hat{\Omega}/2}. \tag{A 6}$$

The solution of (A 5) can be written as

$$P(\hat{\xi}) = \sigma_r P_p(\hat{\xi}) + a_0 P_{h1}(\hat{\xi}) + b_0 P_{h2}(\hat{\xi}), \tag{A 7}$$

where the solutions to the homogeneous equation (P_{h1} and P_{h2}) are calculated using the hypergeometric series around $(1 - \hat{\xi})$ as done by Moase *et al.* (2007),

$$P_{h1}(\hat{\xi}) = {}_2F_1(a, b; 1 + a + b; (1 - \hat{\xi})), \tag{A 8}$$

$$P_{h2}(\hat{\xi}) = (1 - \hat{\xi})^{-a-b} {}_2F_1(-a, -b; 1 - a - b; (1 - \hat{\xi})). \tag{A 9}$$

The values of a and b are calculated through

$$a + b = 1 + \frac{2i\hat{\Omega}}{\gamma + 1} \quad \text{and} \quad ab = \frac{i\hat{\Omega}(2 + i\hat{\Omega})}{2(\gamma + 1)}, \tag{A 10}$$

and the hypergeometric functions ${}_2F_1$ are given by

$${}_2F_1(A, B; C; Z) = \sum_{n=0}^{\infty} \frac{A^{(n)} B^{(n)}}{C^{(n)}} \frac{Z^n}{n!}, \tag{A 11}$$

where $A^{(n)} = A(A + 1)(A + 2) \cdots (A + n - 1)$ is the rising factorial. The particular solution in series of $(1 - \hat{\xi})$ was obtained by Moase *et al.* (2007). It reads

$$P_p(\hat{\xi}) = \frac{-i\hat{\Omega} (\hat{\xi}_r)^{i\hat{\Omega}/2}}{2(\gamma + 1)} \sum_{n=0}^{\infty} c_n (1 - \hat{\xi})^{n+1}, \tag{A 12}$$

where

$$c_n = \frac{c_{n-1}(n + a)(n + b)n! + (-1)^n (1 - n - \frac{1}{2}i\hat{\Omega})^{(n)}}{(n + 1)(n + 1 + a + b)n!}, \quad c_0 = \frac{1}{1 + a + b}. \tag{A 13}$$

As shown by Moase *et al.* (2007), this solution converges for $0 < \hat{\xi} < 2$, which gives a range of Mach numbers from $M > 0$ to $M < \sqrt{4/(3 - \gamma)}$. For a subsonic flow the boundary conditions are the downstream-propagating acoustic wave at the inlet, $w_f^+ = P(\hat{\xi}_{in}) + M_{in}U(\hat{\xi}_{in})$, and the upstream-propagating acoustic wave at the outlet, $w_f^- = P(\hat{\xi}_{out}) - M_{out}U(\hat{\xi}_{out})$. For choked nozzles, the second homogeneous solution behaves like $(1 - \hat{\xi})^{-1-2i\hat{\Omega}/(\gamma+1)}$ near $M = 1$. As P should be regular at this point, this solution should disappear if the throat is located inside the computational domain,

giving $b_0 = 0$. The value of a_0 is obtained by imposing the downstream-propagating acoustic wave at the inlet.

The Mach number of this linear velocity profile nozzle can be calculated as a function of the space coordinate. Using the definition of $\hat{\xi}$,

$$\hat{\xi} = \left(\frac{x}{x_*}\right)^2 = \left(\frac{u}{u_*}\right)^2 = \left(\frac{\gamma + 1}{2}\right) \frac{M^2}{1 + \frac{\gamma - 1}{2}M^2}, \quad (\text{A } 14)$$

and solving for the Mach number,

$$M = \sqrt{\left(\frac{2}{\gamma + 1}\right) \frac{\hat{\xi}}{1 - \left(\frac{\gamma - 1}{\gamma + 1}\right) \hat{\xi}}}. \quad (\text{A } 15)$$

REFERENCES

- BAKE, F., RICHTER, C., MUHLBAUER, B., KINGS, N., ROHLE, I., THIELE, F. & NOLL, B. 2009 The Entropy Wave Generator (EWG): a reference case on entropy noise. *J. Sound Vib.* **574**–598.
- BELL, W., DANIEL, B. & ZINN, B. 1973 Experimental and theoretical determination of the admittances of a family of nozzles subjected to axial instabilities. *J. Sound Vib.* **30** (2), 179–190.
- BLANES, S., CASAS, F., OTERO, J. A. & ROS, J. 2009 The Magnus expansion and some of its applications. *Phys. Rep.* **470** (5–6), 151–238.
- CANDEL, S. 1972 Analytical studies of some acoustic problems of jet engines. PhD thesis, California Institute of Technology.
- CANDEL, S. & POINSOT, T. 1988 Interactions between acoustics and combustion. In *Proceedings of the Institute of Acoustics*, vol. 10, pp. 103–153.
- CASAS, F. 2007 Sufficient conditions for the convergence of the Magnus expansion. *J. Phys. A: Math. Theor.* **40** (50), 15001–15017.
- CROCCO, L. & SIRIGNANO, W. A. 1967 Behavior of supercritical nozzles under three-dimensional oscillatory conditions. In *AGARD*, vol. 117. Butterworth Publications Ltd.
- CULICK, F. E. C. 1988 Combustion instabilities in liquid-fueled propulsion systems – an overview. In *AGARD 72B PEP Meeting, Conference Proceedings 450*.
- CUMPSTY, N. A. & MARBLE, F. E. 1977 The interaction of entropy fluctuations with turbine blade rows; a mechanism of turbojet engine noise. *Proc. R. Soc. Lond. A* **357**, 323–344.
- DOWLING, A. P. 1995 The calculation of thermoacoustic oscillations. *J. Sound Vib.* **180** (4), 557–581.
- DOWLING, A. P. 1997 Nonlinear self-excited oscillations of a ducted flame. *J. Fluid Mech.* **346**, 271–290.
- DOWLING, A. P. & STOW, S. R. 2003 Acoustic analysis of gas turbine combustors. *J. Propul. Power* **19** (5), 751–764.
- DURAN, I., MOREAU, S. & POINSOT, T. 2013 Analytical and numerical study of combustion noise through a subsonic nozzle. *AIAA J.* **51** (1), 42–52.
- GIAUQUE, A., HUET, M. & CLERO, F. 2012 Analytical analysis of indirect combustion noise in subcritical nozzles. *Trans. ASME: J. Engng Gas Turbines Power* **134** (11), 111202.
- GICQUEL, L. Y. M., STAFFELBACH, G. & POINSOT, T. 2012 Large eddy simulations of gaseous flames in gas turbine combustion chambers. *Prog. Energy Combust. Sci.* **38** (6), 782–817.
- GOH, C. S. & MORGANS, A. S. 2011a Phase prediction of the response of choked nozzles to entropy and acoustic disturbances. *J. Sound Vib.* **330** (21), 5184–5198.

- GOH, C. S. & MORGANS, A. S. 2011*b* The effect of entropy wave dissipation and dispersion on thermoacoustic instability in a model combustor. In *Proceedings of the 17th AIAA/CEAS Aeroacoustics Conference, Portland, AIAA-2011-2914*.
- GULLAUD, E., MENDEZ, S., SENSIAU, C., NICOUD, F. & POINSOT, T. 2009 Effect of multiperforated plates on the acoustic modes in combustors. *C. R. Acad. Sci. Méc.* **337** (6–7), 406–414.
- HOWE, M. S. 2010 Indirect combustion noise. *J. Fluid Mech.* **659**, 267–288.
- KUO, C.-Y. & DOWLING, A. P. 1996 Oscillations of a moderately underexpanded choked jet impinging upon a flat plate. *J. Fluid Mech.* **315**, 267–291.
- LEYKO, M., MOREAU, S., NICOUD, F. & POINSOT, T. 2011 Numerical and analytical modelling of entropy noise in a supersonic nozzle with a shock. *J. Sound Vib.* **330** (16), 3944–3958.
- LEYKO, M., NICOUD, F., MOREAU, S. & POINSOT, T. 2008 Numerical and analytical investigation of the indirect noise in a nozzle. In *Center for Turbulence Research, NASA AMES, Proceedings of the Summer Program*, pp. 343–354. Stanford University, USA.
- LEYKO, M., NICOUD, F. & POINSOT, T. 2009 Comparison of direct and indirect combustion noise mechanisms in a model combustor. *AIAA J.* **47** (11), 2709–2716.
- MADHU, P. & KURUR, N. 2006 Fer expansion for effective propagators and Hamiltonians in NMR. *Chem. Phys. Lett.* **418** (1–3), 235–238.
- MAGNUS, W. 1954 On the exponential solution of differential equations for a linear operator. *Commun. Pure Appl. Math.* **7** (4), 649–673.
- MARBLE, F. E. & CANDEL, S. 1977 Acoustic disturbances from gas non-uniformities convected through a nozzle. *J. Sound Vib.* **55**, 225–243.
- MOAN, P. C. & NIESEN, J. 2006 Convergence of the Magnus series. *Tech. Rep.* 0316, La Trobe University.
- MOASE, W. H., BREAR, M. J. & MANZIE, C. 2007 The forced response of choked nozzles and supersonic diffusers. *J. Fluid Mech.* **585**, 281–304.
- MOLER, C. & VAN LOAN, C. 2003 Nineteen dubious ways to compute the exponential of a matrix, twenty-five years later. *SIAM Rev.* **45** (1), 3–49.
- MOTHEAU, E., SELLE, L., MERY, Y., POINSOT, T. & NICOUD, F. 2012 A mixed acoustic–entropy combustion instability in a realistic gas turbine. In *Center for Turbulence Research, NASA AMES, Proceedings of the Summer Program*, pp. 449–458. Stanford University, USA.
- MUTHUKRISHNAN, M., STRAHLE, W. C. & NEALE, D. H. 1978 Separation of hydrodynamic, entropy, and combustion noise in a gas turbine combustor. *AIAA J.* **16** (4), 320–327.
- PICKETT, G. F. 1975 Core engine noise due to temperature fluctuations convecting through turbine blade rows. In *Proceedings of the 2nd AIAA Aeroacoustics Conference, AIAA-1975-528*, Hampton, VA.
- POINSOT, T. & VEYNANTE, D. 2011 *Theoretical and Numerical Combustion*, 3rd edn. (www.cerfacs.fr/elearning).
- RAYLEIGH, L. 1878 The explanation of certain acoustic phenomena. *Nature* 18 July, 319–321.
- RIBNER, H. S. 1953 Convection of a pattern of vorticity through a shock wave. *NACA TN* 2864.
- RIBNER, H. S. 1954 Shock–turbulence interaction and the generation of noise. *NACA TN* 3255.
- RIBNER, H. S. 1987 Spectra of noise and amplified turbulence emanating from shock turbulence interaction. *AIAA J.* **25** (3), 436–442.
- SAKURAI, J. J. & TUAN, S. F. 1985 *Modern Quantum Mechanics*, vol. 1. Addison-Wesley.
- SILVA, C. 2010 Numerical study of combustion noise in gas turbines. PhD thesis, INPT, Toulouse.
- STOW, S. R., DOWLING, A. P. & HYNES, T. P. 2002 Reflection of circumferential modes in a choked nozzle. *J. Fluid Mech.* **467**, 215–239.
- TSIEN, H. S. 1952 The transfer functions of rocket nozzles. *J. Am. Rocket Soc.* **22** (3), 139–143.
- WILCOX, R. M. 1967 Exponential operators and parameter differentiation in quantum physics. *J. Math. Phys.* **8** (4), 962–982.
- WILLIAMS, F. A. 1985 *Combustion Theory*. Benjamin Cummings.
- ZINN, B. T., BELL, W. A., DANIEL, B. R. & SMITH, A. J. 1973 Experimental determination of three-dimensional liquid rocket nozzle admittances. *AIAA J.* **11** (3), 267–272.